Recombinant silk like fusion proteins as next generation matrices for tissue engineering

Teemu Välisalmi

School of Chemical Technology

Thesis submitted for examination for the degree of Master of Science in Technology submitted.

Espoo, 15.11.2018

Supervisor

Prof. Markus Linder

Advisor

M.Sc. Pezhman Mohammadi

Aalto University
School of Chemical
Engineering

Aalto University
School of Chemical
Engineering

Aalto University, P.O. BOX 11000, 00076 AALTO
www.aalto.fi

Abstract of master's thesis

Author Teemu Välisalmi

Title of thesis Recombinant silk like fusion proteins as next generation matrices for tissue engineering

Degree Programme Master's programme in Chemical, Biochemical and Materials Engineering

Major Biotechnology

Thesis supervisor Prof. Markus Linder

Thesis advisor M.Sc. Pezhman Mohammadi

Date 15.11.2018 **Number of pages** 50 **Language** English

Abstract

There is a growing need for tissue transplantations that cannot be met with current biomedical methods. Tissue engineering (TE) is a new interdisciplinary field that aims to construct viable tissues by utilizing artificial tissue scaffolds and bioreactors. To achieve this cells need to be provided with various stimuli that are present in their natural surroundings, the extracellular matrix (ECM). The most important properties of ECM are absence of cytotoxicity, biocompatibility, biodegradability and mechanical properties, which should be adapted in the scaffold biomaterial. Other necessary properties are zero risk of pathogens, versatile manufacturing and inexpensive production. Currently there is no such material available and thus TE is searching for new potential biomaterials, one of them being spider silk proteins.

Spider silk proteins have exceptional mechanical properties, including no cytotoxic effects, biocompatibility and biodegradability. In addition, spider silks can be manufactured into different morphologies, such as fiber meshes or foams. However, cannibalistic nature of spiders and low production of silk protein make harvesting of native silk very inefficient. Recombinant production can be utilized to overcome these issues and previous research has shown that recombinant spider silk proteins are suitable for TE, and that the biocompatibility can be improved by introducing bioactive molecules to the protein structure via genetic engineering.

Three silk like fusion proteins based on spidroin ADF3 by *Araneus diadematus* were produced with cytotoxic lipopolysaccharide free *Escherichia coli* strain. The silk constructs were CBM-ADF3-CBM, CBM-ADF3-FB_H-Crys and Crys-ADF3-FB_H-Crys, where CBM is cellulose binding module from *Ruminiclostridium thermocellum*, FB_H is heparin binding site from fibronectin and Crys is gamma crystallin D from *Homo sapiens*. Cytotoxicity and biocompatibility in forms of cell viability and adhesion were tested with human dermal fibroblast (HDF) cultivations on silk films, and the results showed notable improvement in cell viability when replacing CBM with Crys. In addition, there was no signs of cytotoxicity. Cell adhesion was hardly improved with addition of binding site in CBM-ADF3-FB_H-Crys suggesting inaccessibility of the site or non-compatibility with HDF. Results of Crys-ADF3-FB_H-Crys were comparable with conventional material gelatin.

Keywords Tissue engineering, silk, spider, biocompatibility, fusion protein, recombinant

Tekijä Teemu Välisalmi

Työn nimi Rekombinantti silkin kaltaiset fuusioproteiinit seuraavan generaation matrikseina kudosteknologiassa

Koulutusohjelma Master's programme in Chemical, Biochemical and Materials Engineering

Pääaine Biotekniikka

Työn valvoja Prof. Markus Linder

Työn ohjaaja M.Sc. Pezhman Mohammadi

Päivämäärä 15.11.2018 **Sivumäärä** 50 **Kieli** englanti

Tiivistelmä

Kudossiirrosten kysyntä kasvaa jatkuvasti eikä nykyiset lääketieteen menetelmät kykene vastaamaan tähän tarpeeseen. Kudosteknologia on uusi monitieteellinen ala, jonka tavoitteena on kasvattaa elinkelpoisia kudoksia käyttämällä keinotekoisia tukiverkkomateriaaleja ja bioreaktoreita. Tämän saavuttaakseen solut tarvitsevat samankaltaisia ärsykkeitä kuin niiden luonnollisessa elinympäristössä, soluväliaineessa. Väliaineen tärkeimmät ominaisuudet ovat biosopivuus, biohajoavuus, sytotoksisuus ja mekaaniset ominaisuudet, jotka tulisivat olla myös tukiverkko-materiaalissa. Lisäksi muita tarpeellisia ominaisuuksia ovat olematon patogeenien riski, tuotteen muotoilumenetelmät ja edullinen tuotanto. Tällä hetkellä vastaavaa materiaalia ei ole saatavilla, joten uusia lupaavia biomateriaaleja tutkitaan jatkuvasti, joista yksi on hämähäkin silkkiproteiini.

Hämähäkin silkkiproteiineilla on erinomaiset mekaaniset ominaisuudet, ne eivät aiheuta sytotoksisuutta ja ovat biosopivia sekä biohajoavia. Lisäksi hämähäkin silkki voidaan valmistaa eri muotoihin, kuten kuituverkoksi ja vaahdoksi. Kuitenkin, hämähäkkien kannibalisminen luonne ja alhainen silkin tuotanto tekevät silkin keräyksestä erittäin epätehokasta. Rekombinanttituotantolla tuotto on skaalattavissa ja aikaisemmat tutkimukset ovat osoittaneet, että rekombinantti hämähäkin silkki soveltuu kudosteknologian käyttötarpeisiin, ja että biosopivuutta voi parantaa lisäämällä bioaktiivisia molekyylejä silkkiproteiinin rakenteisiin geenitekniikan avulla.

Tässä diplomityössä tuotettiin kolmea silkin kaltaista fuusioproteiinia, jotka pohjautuvat ADF3 silkkiproteiiniin (*Araneus diadematus*): CBM-ADF3-CBM, CBM-ADF3-FB_H-Crys ja Crys-ADF3-FB_H-Crys, jossa CBM on selluloosakiinnitysmoduuli (*Ruminiclostridium thermo-cellum*), FB_H on solukiinnityspaikka fibronektiinistä ja Crys on gamma D krystalliini (*Homo sapiens*). Tuotto tehtiin *Escherichia coli* kannalla (ClearColi BL21), joka ei tuota sytotoksisia lipopolysakkarideja. Silkin sytotoksisuus, solukiinnitys ja -elinkelpoisuus ominaisuudet testattiin ihokudossolukasvatuksilla (HDF) silkkiproteiinifilmeillä. Tulokset osoittivat huomattavan parannuksen soluelinkelpoisuudessa, kun CBM vaihdettiin krystalliiniksi. Sytotoksisia vaikutuksia ei huomattu. Solukiinnitys ei parantunut oletettavasti kiinnityspaikan lisäyksessä, mikä viittaa epäsopivuuteen HDF:n kanssa tai paikan luoksepääsemättömyyteen. Crys-ADF3-FB_H-Crys tulokset olivat verrattavissa yleisesti solukasvatuksissa käytettyyn gelatiiniin.

Avainsanat kudosteknologia, silkki, hämähäkki, biosopivuus, fuusioproteiini, rekombinantti

Preface

I would like to thank Markus Linder (Prof.) for the opportunity to work in Biomolecular Materials research group, Pezhman Mohammadi (M.Sc) for the excellent guidance, Sesilja Aranko (PhD) for the thesis topic and silk construct designs, Apeksha Damania (PhD) for the help with cell culturing and biocompatibility assays and Kai Liu (PhD) for performing the contact angle measurements.

Espoo, Finland
15.11.2018

Teemu Välisalmi

Table of contents

Symbols and Abbreviations

2D	2-dimensional
3D	3-dimensional
ADF3	Major ampullate spidroin 1 (*Araneus diadematus*)
ANOVA	Analysis of variance
BSA	Bovine serum albumin
CA	Contact angle
CBM	Cellulose binding module
Crys	Gamma D crystallin (*Homo sapiens*)
DAPI	4′,6-diamidino-2-phenylindole
DMEM	Dulbeccos's modified eagles medium
DMSO	Dimethyl sulfoxide
DTT	Dithiothreitol
ECM	Extracellular matrix
FA	Formaldehyde
FB_H	Heparin binding site from fibronectin
FDA	United States Food and Drug Administration
FPLC	Fast protein liquid chromatography
FTIR	Fourier-transform infrared spectroscopy
GAG	Glycosaminoglycan
HDF	Human dermal fibroblast
IID	Independent and identically distributed
in vivo	In the glass
in vitro	Within the living
IPTG	Isopropyl β-D-1-thiogalactopyranoside
IR	Infrared spectroscopy

LAL	Limunus amebocyte lysate
LB	Lysogeny broth
LPS	Lipopolysaccharide
MaSP	Major ampulla spidroin
MTT	3-(4,5-dimethylthiazol-2-yl)-2,5-diphenyltetrazolium bromide
NADH	Nicotinamide adenine dinucleotide
OD	Optical density
PAGE	Polyacrylamide gel electrophoresis
PBS	Phosphate-buffered saline
PCR	Polymerase chain reaction
PFA	Polyformaldehyde
PGA	Polyglycolide
PLLA	Poly-l-lactic acid
RGD	Arginine-glycine-aspartate
RSSP	Recombinant spider silk protein
RT	Room temperature
SD	Standard deviation
SDS	Sodium dodecyl sulfate
SEM	Scanning electron microscope
TE	Tissue engineering

1 Introduction

Currently skin and organ damages can be treated with transplantation treatments, where the transplanted tissue originates from the same patient or from another individual. While these methods are widely used in medical science, they have major limitations such as risk of rejection, applicability for severe wounds and availability of enough transplants for all patients. Tissue engineering (TE) is a new interdisciplinary field combining knowledge from biomedical and engineering sciences aiming to solve these problems by constructing viable tissues with the use of artificial tissue scaffolds. In general, relevant cell line(s) would be seeded onto the artificial scaffold matrix and grown in bioreactor while providing sufficient stimuli for the cells until the formed tissue is fully functional and ready for implantation. The natural environment of the cell, extracellular matrix (ECM), can be investigated to get an understanding of the required properties for the scaffold material, and this would suggest that the most important are absence of cytotoxicity, biocompatibility, biodegradability and ECM-like mechanical properties, such as high tensile and compressive strength. Also, in engineering point of view low cost and versatile manufacturing are required for commercial applications. [1]

Current scaffold materials can be divided into three groups; ceramics, synthetic polymers and natural polymers. While these materials are used in the biomedical science, all have their shortcomings; e.g. ceramics have poor biodegradability and limited manufacturing, synthetic polymers are not biocompatible, and natural materials, such as ECM extracts from mammalian cells are susceptible to pathogens that are difficult to detect, and tend to be expensive. Thus, TE field is searching for new biomaterials and many promising materials are already under development, one of them being spider silks. They have remarkable mechanical properties, such as combination of high tensile strength and elasticity, while they are also biodegradable and fairly biocompatible, and do not cause cytotoxic effects with mammalian cells. The spider silk threads are composed of silk proteins that have long central part with repetitions of crystalline and amorphous regions, flanked with small terminal domains. In silk fibers the crystalline regions form β-sheets, which are responsible for the mechanical strength while elasticity comes from the amorphous regions. The terminal units are believed to control fiber formation from liquid to solid. [2]–[5]

While the spider silks have exceptional properties, production has been problematic. Harvesting spider silk from spiders is inefficient due to their cannibalistic nature and low silk thread yield. Recombinant production of different silk proteins has been tested with various prokaryotes and eukaryotes, such as *Escherichia coli*, *Pichia pastoris* and *Bombyx mori* cells, but long and repetitive sequence of spider silks causes issues with polymerase chain reactions (PCR) and

expression system of the hosts, especially in prokaryotes and lower eukaryotes. Also, spider silks are prone to aggregate and have high content of certain amino-acids exhausting amino-acid and tRNA reserves of the host resulting in poor yields. If the silk is produced for biomedical uses, pathogenicity and cytotoxicity are other factors that affect the suitability of the host organisms; e.g. mammalian cells can harbor undetectable cryptic viruses and Gram-negative bacteria, such as *E. coli* release cytotoxic lipopolysaccharides (LPS) that are difficult to remove from the silk product. While biotechnological production of spider silk has significant limitations, many approaches have been implemented to overcome these issues, such as producing shorter spider silks, engineering of the central part and overexpression of bottlenecking amino-acid reserves. [5]–[8]

Thus, recombinant spider silk proteins (RSSP) seem to be suitable for TE and some research has already been done on this topic. RSSP rS1/9 (94 kDa), an analogue of *Nephila clavipes* spidroin 1, was tested in vivo and in vitro studies by Moisenovich et al., showing good biocompatibility, biodegradability and promotion of tissue growth [9]. RSSPs pNSR-16 and pNSR-32 (102 and 196.6 kDa), both containing an Arg-Gly-Asp (RGD) cell adhesion site from fibronectin, were tested in vivo experiments (rat burn wound) and the results suggested suppression of inflammatory effects and good biocompatibility, with no significant difference to commercially used collagen foam [10]. RSSP 4RepCT was constructed by Stark et al. and it consisted of four repetitions of crystalline and amorphous regions with C terminal domain from major spidroin 1 of *Euprosthenops australis* resulting to length of 23.8 kDa [11]. 4RepCT was tested in vivo with rat wounds and the results showed good biodegradability and biocompatibility supporting growth of vascularized tissue, albeit with slight inflammatory effect [12]. Widhe et al. studied the effect of adding RGD binding site to 4RepCT and in vitro experiments showed notable improvement in cell adhesion and viability compared to the original 4RepCT [13]. These results support the suitability of RSSPs in TE, and that the properties can be enhanced with genetic engineering.

The aim of this thesis was to evaluate cytotoxicity and biocompatibility of silk like fusion proteins based on ADF3, major ampullate spidroin 1 by *Araneus diadematus*, and draw structure-function relationships between the constructs and compare them to conventional matrix materials. Three silk constructs were produced with cytotoxic LPS free *E. coli* strain (ClearColi BL21). The silk constructs were CBM-ADF3-CBM, CBM-ADF3-FB_H-Crys and Crys-ADF3-FB_H-Crys, where CBM is cellulose binding module from *Ruminiclostridium thermocellum*, ADF3 is gland silk fibroin 3 from *A. diadematus* without terminal units, FB_H is heparin binding site from fibronectin and Crys is gamma crystallin D from *Homo sapiens*. Gamma crystallin is an extremely stable and soluble protein found in human eye nerve cells [14].The hypothesis was that replacing CBM with gamma crystallin increases biocompatibility while retaining high solubility, and addition of cell binding site

increases cell adhesion. Cytotoxicity of the silk constructs was tested with human dermal fibroblast (HDF) two dimensional (2D) cultivations. Biocompatibility with HDF (2D) was tested in forms of cell viability and cell adhesion with metabolic activity assay (MTT) and cell adhesion assay, respectively. The results were compared to conventional material gelatin, and structure-function relationships for replacement of CBM with crystallin and presence of adhesion site were studied. While useful, implementation of 3D scaffolds, modification of silk films with kosmotropic salts and additional silk constructs were beyond of the scope of this thesis.

2 Background / Literature review

This literature review goes through some key aspects of what to consider when designing functionalized silk proteins for tissue engineering. The first part covers relevant biological background: structure of extracellular matrix, general properties required in scaffold materials, mammalian cell adhesion, current scaffold biomaterials and how to functionalize them. The second part covers spider silk proteins in general, previous research in spider silk functionalization and novelty of silk-like fusion proteins that were used in this thesis.

2.1 Biological background

2.1.1 Extracellular matrix and scaffold material properties

The extracellular matrix (ECM) is a mixture of extracellular proteins secreted by the local cells (Figure 1). The matrix has various functions; it provides a structural support for the cells, contains binding domains for adhesion receptors, and binds soluble growth and other signaling factors. These factors affect the cell behavior, such as differentiation, polarity and migration of the cells. The structure and content of ECM varies between cell types; tendons have high ECM content while organs have little of it, and epithelial rich areas tend to have highly vascularized ECM that contain mostly collagen I while basement membrane contain typically collagen IV, laminin and entactin. [15], [16]

The ECM proteins are generally large and complex, and contain repeats of different highly conserved domains [15]. While the domains can be found in other protein families, the arrangement of the domains are unique to ECM proteins. This can be used to identify ECM proteins from protein databases resulting in a list of proteins that comprises 1-1.5% of mammalian proteome. Main components of the list are glycoproteins (~200), collagen subunits (43) and proteoglycans (~40). [17]

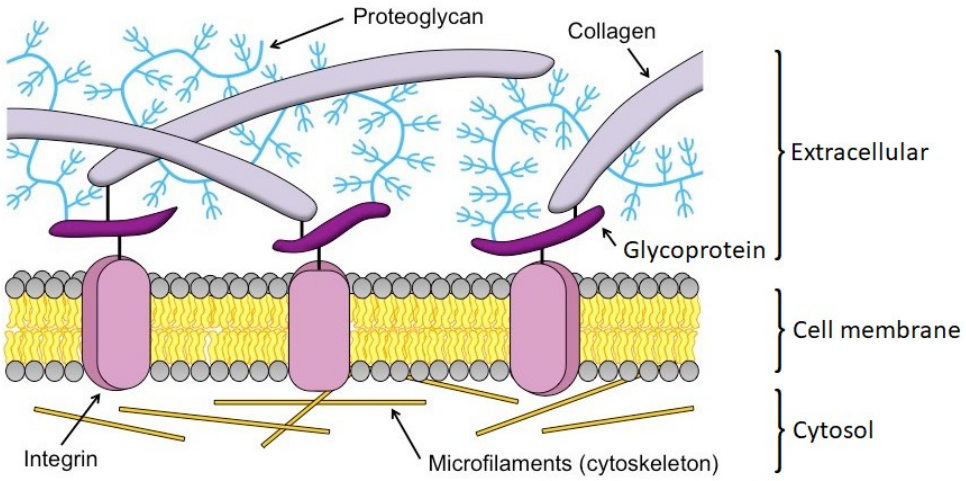

Figure 1. Extracellular matrix (ECM) with attachments to cell. Main components of ECM are glycoproteins, proteoglycans and collagens. Cells attach to ECM via integrins. Modified from: [18].

Glycoproteins are proteins that contain one or more oligosaccharide chains. The oligosaccharide chains are generally relatively short and branched, and attached covalently to a side chain of the protein during post-translational modification. The sugar chains have various effects on the protein, such as making it more resistant to proteases, assisting in folding, and modifying antigenic and functional properties. ECM glycoproteins have multiple functions, such as ECM assembly, binding growth factors, cell adhesion and signaling. The most well-known and abundant glycoprotein is fibronectin, which is composed of two large subunits that are linked with sulfide bonds. It has binding sites for cells, matrix fibers, various signaling factors, and it can serve as a linkage between other ECM proteins and cell membrane via cell adhesion sites. The most well-known cell adhesion site in fibronectin is RGD tripeptide (Arg-Gly-Asp), which is often used in functionalization of scaffold biomaterials. In addition, fibronectin has complex functions, such as shifting from soluble to insoluble fibers between cells and ECM when under tension, and containing buried integrins that are only available after digested by proteases. [17], [19]

The structural strength of ECM is provided by collagens, which can be divided into two sub-groups by their ability to form fibrils; fibrillar and non-fibrillar collagens. Formations of different collagens vary significantly, but they are all recognized by the presence of three polypeptide chains (α chains), and a tripeptide motif Gly-X-Y, X and Y being any amino acid. In a typical collagen, the three α chains contain numerous repetitions of the tripeptide motif, which allow the chains to form triple-helical structures (Figure 2). These triple-helical structures form micro fibrils that bundle into collagen fibers. The most abundant fibrillar collagen is collagen I, which is found in wide variety of cell types, such as tendon and vasculature. It has two identical α chains and one distinct α chain, each chain consisting around 340 repeats of Gly-X-Y, flanked by short non-helical regions. Unlike many other collagens, the repeats are mainly uninterrupted resulting in rigid triple helix formation with higher tensile strength. The most well-known non-fibrillar collagen is collagen IV, which is mainly found in basement membranes alongside with laminin and entactin. Collagen IV has interruptions in its Gly-X-Y repeats making it flexible, and it forms an open network -like structure that connects with other membrane components. [17], [20]

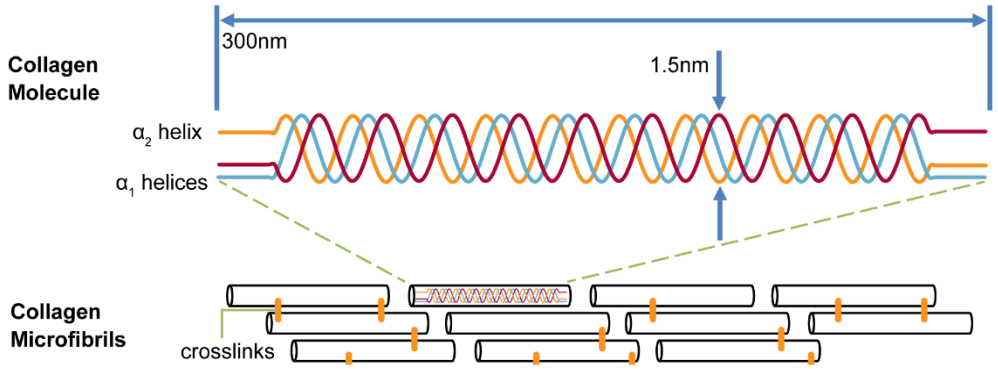

Figure 2. Collagen fiber structure. Core components of collagen are three different polypeptide chains (α chains) that form triple-helical structures, which crosslink with each other bundling into collagen micro fibrils. Modified from: [21].

Like glycoproteins, proteoglycans are also proteins with one or more sugar side chains. The difference is that significant fraction of the side chains are unbranched glycosaminoglycans (GAG), which are large and highly charged polysaccharides. GAGs tend to occupy huge volume relative to their mass, and bind cations creating osmotic pressure allowing ECM to endure compressive forces. The side chains can contribute up to 95% of the protein's total weight, resulting in massive molecules. Certain GAGs can also bind to growth factors, collagen and various glycoproteins. [17], [19]

In summary, ECM is a complex mixture of proteins, which all play some part in providing suitable living conditions for the cells. Thus, designing one polymer to mimic ECM is far from trivial, but it is possible to target the most important properties present in ECM. The obvious properties shown in this chapter are mechanical properties, such as structural strength of collagen and compressive strength of GAGs, and biocompatibility from adhesion sites, growth and other signaling factors. Another property is cytotoxicity meaning that the material is not toxic and it is not recognized as foreign, which would cause inflammatory effect and potentially be rejected by the cells. Also, biodegradability is important allowing the cells to degrade the matrix if needed. Considering in vivo use of scaffold materials, slow continuous degradation to non-harmful components would be preferred. Finally, porous matrix with sufficient pore size is desirable to allow thorough migration of cells. [22] Thus, the structure of the material needs to 3-dimensional, such as fiber mesh or foam, and its pore size should be controllable with different fabrication methods. Out of the given properties biocompatibility is the most complex, and while ideally all of the signals should be provided, it is more realistic to target the most important and well-known attributes. Thus, often cell adhesion is the first attribute to be enhanced.

2.1.2 Cell adhesion

Cell adhesion is fundamental for multicellular organisms as the cells must cohere to keep the organized multicellular structure intact. The attachments affect development of the structure by controlling orientation and behavior of the cell's cytoskeleton. There are cell-cell and cell-ECM junctions, and while both are important when considering formation of functional tissue, cell-ECM is focused here to provide short introduction on cell adhesion sites at ECM. [19]

Cell-ECM junction occurs between an adhesion receptor at cell membrane and a ligand at ECM. The adhesion receptors are transmembrane proteins that belong to two transmembrane superfamilies; cadherins and integrins, which are mainly responsible of cell-cell and cell-ECM anchoring junctions, respectively. Thus, integrins and their respective ligands are in high interest when investigating potential mammalian cell adhesion sites. Integrins consist of α- and β-transmembrane protein subunits (Figure 3), which have small cytoplasmic domains linking to cytoskeleton of the cell and large extracellular domains attaching to ECM ligands or other counter-receptors at the interface of the α- and β-subunit. 24 different α-β integrin combinations formed from 18 α and 8 β subunits have been identified in mammalian genomes as of 2006. Most integrins bind to wide variety of ligands with different affinities and vice versa; e.g. tripeptide RGD ligand found in fibronectin is known to bind to at least 8 integrins. Other RGD containing proteins can compete with fibronectin in cell adhesion and even just the RGD tripeptide without other amino-acids can bind to integrins. However, not all proteins with RGD sequence mediate cell attachment. The site can be buried inside the folded protein or present in non-compatible form, and thus inaccessible to integrins. Also, the presentation of the RGD sequence affects the affinity to different integrins; e.g. large fibronectin fragments with RGD bind with high affinity to $\alpha_5\beta_1$ integrin while smaller ones are preferred by vitronectin receptor $\alpha_V\beta_3$ integrin. [19], [23], [24]

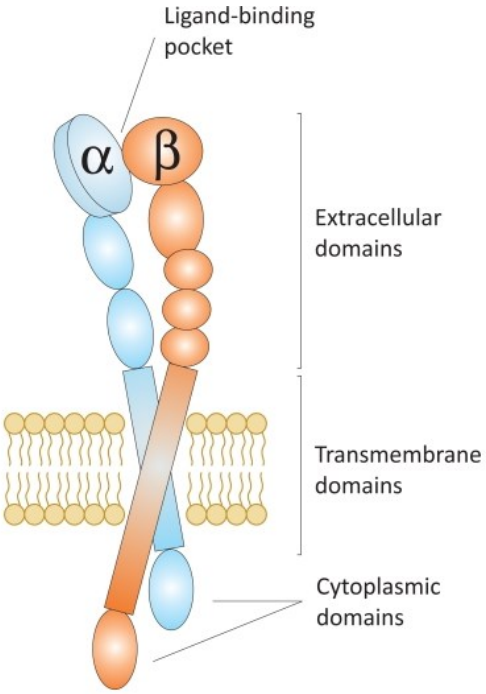

Figure 3. Integrin in unligated state. Integrins are composed of α- and β-transmembrane protein subunits that have cytoplasmic, transmembrane and extracellular domains. The yellow layer is cell membrane. Modified from: [25].

While RGD is the most well-known adhesion site, it is not necessary always the best choice for functionalization of scaffold materials. RGD has been noted to require much higher surface densities to achieve similar binding properties compared to other more specific ligands. New adhesion sites can be identified with advanced methods such as surface arrays with self-assembling peptide monolayers. It can test wide variety of adhesion sites with different surface densities simultaneously. For example heparin adhesion sites FHRRIKA and GWQPPARARI were identified with surface array and both were noticed to mediate binding to human embryonic cells with better properties than RGD. [26], [27]

2.1.3 Current biomaterials & functionalization

Biomaterials are defined as materials that interact with biological systems and influence their biological processes with the aim to regenerate functional tissue. The current biomaterials can be divided into three groups: ceramics, synthetic materials and natural materials. The properties of the groups are summarized in Table 1, and some materials with United States Food and Drug Administration (FDA) or similar approval are given as an example. In addition to these groups, blends of different groups can be used to tailor the properties, e.g. natural ECM polymers tend to have poor mechanical properties, which can be reinforced with synthetic polymers that by themselves lack the bioactivity. [1]

Table 1. Biomaterial groups with some materials as an example.

Group	Material	Pros	Cons	Ref.
Ceramic	Hydroxyapatite	Biocompatibility (bone tissue), mechanical properties, cheap	Limited fabrication, poor degradation, limited use	[1]
	Bioglass 45S5 (collagen blend)	Biocompatibility (bone tissue), mechanical properties, proteolytic degradation	Limited fabrication, limited use, expensive, pathogen risk	[28]
Synthetic polymer	Polyglycolide, polylactides	Mechanical properties, cheap, fabrication, hydrolytic degradation	Biocompatibility, acidic degradation	[29]
	Polydioxanone	Cheap, fabrication, hydrolytic degradation, monofilament sutures	Biocompatibility, acidic degradation, low modulus	[29]
Natural polymer (ECM extract)	Collagen	Natural biocompatibility, proteolytic degradation	Mechanical properties, expensive, batch-to-batch variation, pathogen risk	[1], [30]
	Gelatin (partially hydrolyzed collagen)	Natural biocompatibility, proteolytic degradation, strong hydrogels	Mechanical properties, fast degradation, batch-to-batch variation, pathogen risk	[30]
	Matrigel	Excellent natural biocompatibility, proteolytic degradation	Mechanical properties, very expensive, batch-to-batch variation, pathogen risk, fabrication	[31]
Natural polymer (non-ECM)	Alginate, chitosan (polysaccharides)	Mechanical properties (decent), biocompatibility, proteolytic degradation, cheap		[32], [33]
	Silk worm silk (protein)	Mechanical properties (excellent), biocompatibility, proteolytic degradation (slow), easy functionalization	Structure formation not well understood	[34]

Ceramics, such as hydroxyapatite and tri-calcium phosphate, have high mechanical stiffness, low elasticity and brittle surface. Ceramics have been mainly used in orthopedics due to their compatibility with bone tissue: they share chemical and structural similarities with native bone, which allows good interaction with osteogenic cells enhancing their differentiation and proliferation. However, the major disadvantages are negligible biodegradation with exception of a few bioceramics, and limited fabrication. [1] Biological properties have been improved

by blending biodegradable hydroxycarbonate (bioglass) with bioactive natural polymer collagen. The combination is called Bioglass 45S5, which has been used in over million bone defect surgeries. [28]

Synthetic polymers, such as certain polymerized forms of lactic acid (polylactide), have good mechanical properties and low production costs, and the architecture of the scaffold is highly controllable. Most of the synthetic polymers are degradable via chemical hydrolysis and not affected by cell-triggered proteases. Thus, degradation does not vary between patients, which is often preferred over the randomness of natural degradation. However, chemical hydrolysis of many synthetic polymers, such as poly-l-lactic acid (PLLA) and polyglycolide (PGA), form carbon dioxide as a byproduct of degradation that lowers the pH of its surroundings inducing necrosis. Unlike ceramics and natural polymers, biocompatibility of the synthetic polymers tends to be very low, which leads to poor interaction with cells and increases the chance of inflammatory response. Nevertheless, many synthetic polymers, such as PGA, polylactides and polydioxanone have been widely used in less demanding surgical treatments (e.g. sutures). [1], [22], [29]

Natural polymers refer to polymers that are produced in nature, and thus the group contains wide range of possible materials with different properties. The major subgroup of natural polymers with biomedical applications is animal derived ECM extracts, such as collagen from animal skins and Matrigel, mixture of ECM proteins from mouse sarcoma cells. Generally ECM extracts have very favorable biological properties including natural biodegradation rate and exceptional biological activity that promotes cell interactions. The downsides are batch-to-batch variations, difficult fabrication, insufficient mechanical properties for load-bearing applications, too rapid and uncontrollable degradation for some applications and expensive production. In addition, major problem with animal derived cell extracts are risk of pathogens since they can harbor cryptic viruses and other undetectable diseases that can infect the patient. Nevertheless, the superior biological properties outweigh the downsides and ECM extracts are the current go to choice for many tissue engineering applications. To avoid risk of pathogens, some recombinant ECM proteins can be produced with prokaryotes and lower eukaryotes, e.g. collagen has been produced with bacterial host, albeit with some difficulties in large-scale production due to absence of eukaryotic post-translational modification. Non-ECM natural polymers such as chitosan, alginate and silk worm silk (fibroin) have been designed to excel in areas that are lacking in ECM extracts. They are generally easy produce without batch-to-batch variation and fabricate into different morphologies, cheap and have decent mechanical properties, but compared to ECM extracts the biological activity is mediocre at best. The use of alginate, chitosan and fibroin have been approved for some surgeries by FDA. [1], [22], [33]–[35]

2.1.4 Functionalization of biomaterial

Biomaterials can be functionalized by adding bioactive domains to enhance biocompatibility and other biological properties. Commonly used techniques for altering surface of biomaterial are physical adsorption, covalent immobilization and encapsulation. In physical adsorption biomaterial is dipped in liquid containing bioactive molecules which adhere onto the biomaterials driven by their affinities. This can be enhanced by increasing the wettability of the biomaterial, but since adsorption is based on weak interactions, the method is inefficient and the bioactive molecules can diffuse rapidly when the surrounding medium is changed. In encapsulation bioactive molecules are encapsulated inside the biomaterial and released slowly to the medium while protecting the capsulated molecules from degradation, which is especially useful in drug carrier applications. Covalent immobilization can be used to induce a strong coupling between functional groups of the biomaterial and bioactive molecule, such as carboxylic and amine group. Other reactive functional groups needs to be protected prior to the immobilization, followed by removal of the protection, which might affect biological activity of the materials. Also, the method has poor controllability and with multiple functional groups the exact coupling locations cannot be pre-determined. However, by using recombinant proteins and gene engineering it is possible to design the protein-based biomaterial to contain various bioactive domains at specific locations, and it would eliminate the need of chemical treatments. The DNA sequence of protein biomaterial is fused with DNA of the bioactive molecule, and the new DNA is inserted to an expression system, produced and purified. There are limits to this method since modification of the biomaterial can have various unwanted effects, such as incorrect protein folding, disruption in biomaterial matrix structure, inaccessibility of the bioactive molecule or poor production yield. [36], [37]

Some already tested strategies in functionalization of protein-based biomaterials are addition of ligands for integrins, such as RGD and REDV peptides to enhance cell adhesion and recognition sites for proteases to improve biodegradability. Other possible modifications are addition of antimicrobial domains to prevent bacteria adhesion, binding domains for certain ions e.g. calcium for teeth implants, and fusion with full or fragments of bioactive proteins, such as fibronectin and various growth factors. [36], [37] For synthetic materials physical adsorption and encapsulation are often easier to implement than covalent immobilization. As an example biocompatibility of synthetic polymer PCL has been enhanced by dissolving bioactive heparin into water and then mixing it with methanol and DCM. This solution was loaded to PCL matrix, which showed positive results in preventing binding of unwanted cell types, without causing inflammatory response. [38]

2.2 Spider silk and its functionalization

Spiders have the ability to produce a variety of silk threads suitable for different purposes, such as weaving elastic webs for catching prey and strong safety lines to escape predators. The silk threads are composed of proteins and each silk type has unique mechanical properties. Dragline silk that is used in web frames and safety lines is known to have exceptional tensile strength and elasticity, and thus it has been the main focus in spider silk research. The silk dope is produced in the glands of the spider, and the major ampullate gland is responsible of dragline silk production (Figure 4). The protein components of dragline silk, spidroins, are formed in epithelial cells located in the glands tail and partly in the sac (purple area in Figure 4) and secreted into the sac. Spidroins are stored there in soluble form at very high concentrations (up to 50 %-w/v) and they are converted into solid fibers via phase separation in the funnel and spinning duct (grey area in Figure 4). During the conversion water and chaotropic ions, sodium and chloride, are extracted and simultaneously kosmotropic ions potassium and phosphate are added, which also increases acidity from neutral pH to below pH 6. One major enzyme in this process has been identified to be carbonic anhydrase that extracts water and lowers pH by catalyzing conversion of CO_2 and H_2O to H^+ and bicarbonate (HCO_3^-). In addition, spider pulls the silk thread from the end of the spinning duct, spinneret, applying mechanical stress on the silk dope in the spinning duct, which is believed to induce formation of orientated fibers, together with the change of pH and other ionic concentrations. [5], [39]

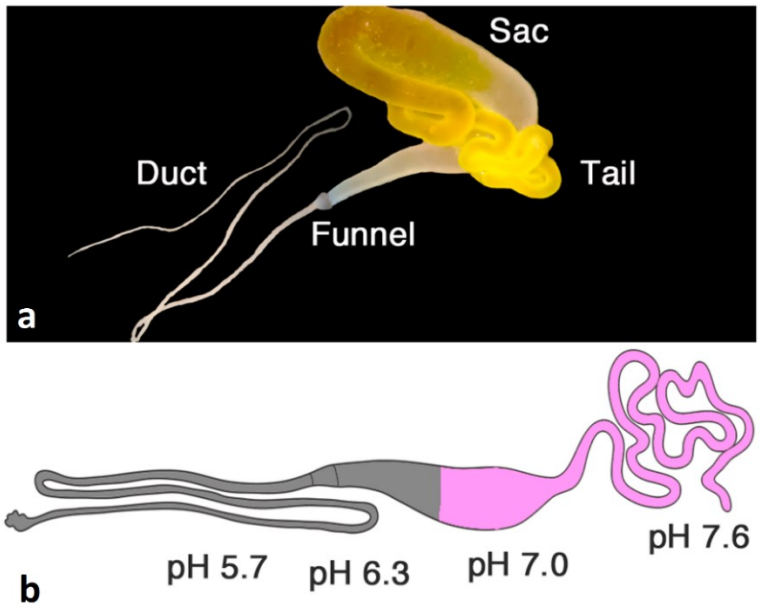

Figure 4. Major ampullate gland (a), with schematic version including approximated pH values (b). Spidroins are secreted in the purple part and the silk dope is converted from liquid to insoluble fibers in the grey area. Modified from: [39].

Dragline silks are mainly composed of two silk proteins; major ampulla spidroins (MaSP) 1 and 2. They are structurally similar consisting of long repetitive central part (>200 kDa) with hydrophobic polyalanine motifs and amorphous hydrophilic glycine-rich segments, and non-repetitive terminal domains. In silk fibers polyalanine blocks form β-sheets that stack into crystalline regions resulting in high tensile strength while extensibility of the fibers comes from the amorphous regions. Due to this combination, dragline silk can absorb exceptional amount of energy before deforming (toughness) exceeding other man-made materials, such as Kevlar. The non-repetitive C- and N-terminal domains are assumed to assist in formation of proper fibers from liquid silk dope and both domains are highly conserved in MaSPs indicating their necessity. [3], [40]

In addition to exceptional mechanical properties of spidroins, they have also been shown to exhibit favorable properties in vivo and in vitro experiments, e.g. supporting regeneration of peripheral nerves, suggesting absence of cytotoxicity and sufficient biocompatibility. Also, silk fibers are susceptible to some mammalian proteases, such as chymotrypsin that cleaves the amorphous regions allowing slow degradation in vivo. Silk proteins have been shown to lose their tensile strength in one year and disintegrate in two years in vivo. Furthermore, spider silk can be processed into different morphologies, such as hydrogels, films and fiber meshes. In case of recombinant spider silk proteins (RSSP) the mechanical properties can be tuned by altering the conversion from liquid silk dope to fiber, and the biotechnological production is scalable allowing production of large quantities with reasonable prices compared to mammalian derived ECM-proteins without risk of pathogens. Thus, spider silk fulfils the requirements for scaffold material that were mentioned previously. [3], [4], [41], [42]

Compared to currently used biomaterials, spidroins are very similar with sericin-free fibroins, with the exception of better mechanical properties. Polysaccharide-based non-ECM natural polymers are cheaper to produce, but lack the ease of functionalization and mechanical properties. ECM extracts have better biocompatibility, but are much more expensive, difficult to fabricate, include risk of pathogens and batch variation, and have inferior mechanical properties. While ceramic implants seems to be quite different, the macromolecules of native bone are mainly composed of collagen network (~30 % of bone mass) [43]. Thus, the network could be replaced with spidroin mesh and mineralized with hydroxyapatite nanoparticle crystals resulting in bone implants with improved load-bearing properties [43]. Synthetic polymers can achieve mechanical properties close to spidroins [29] and they are cheaper to produce. However, they lack biocompatibility, targeted functionalization and natural degradation. Thus, spider silk seems to be a very promising biomaterial, but some major issues still needs to be solved. Conversion from liquid silk dope to solid fiber is not well understood preventing RSSP fibers achieving similar mechanical properties with native

dragline silk, and more advanced biocompatibility is required for formation of functional tissue both in vitro and in vivo. [3], [4]

There has been some previous research on functionalization of RSSP. Various cell binding sites have been tested with different RSSPs. Stark et al. constructed a short RSSP (23.8 kDa) 4RepCT that consisted of four repetitions of crystalline and amorphous regions with C terminal domain from major spidroin 1 of *Euprosthenops australis* [11]. Widhe et al. studied the effect of adding RGD sequence from fibronectin type III module 10 to 4RepCT with three different versions; XTGRGDSPAX, where the X's were replace with cysteines (FN_{CC}), valine and serine (FN_{VS}), and serines (FN_{SS}). RGD with two cysteines were assumed to form disulfide bond resulting in a hairpin loop resembling the structure of RGD in native fibronectin, and the other two conformations were used as controls. Early cell adhesion (1 hour) to the silk films was tested with endothelial cells, mesenchymal stem cells and keratinocytes. RGD silk films promoted cell adhesion compared to the unmodified 4RepCT and FN_{CC} showed significant improvement to other RGD silk film, indicating the importance of the conformation of RGD. [13] Wohlrab et al. studied addition of GRGDSPG to eADF4 RSSP. The modification did not affect secondary structure, water contact angle or surface toughness of the silk films, and cell adhesion to BALB/3T3 mouse fibroblasts was significantly improved [44]. The same material was used by Schaht et al. to produce hydrogel (3 %-w/w) and the RGD modified version showed significant improvement in cell adhesion with all tested cell lines (fibroblast, myoblast, HeLa cell, osteoblast, and keratinocyte). In addition, they tested 3D printing of hydrogels seeded with fibroblasts, which showed sufficient viability, albeit slightly lower than commonly used alginate. However, the mechanical properties of the silk hydrogel was better than the alginate, which requires toxic thickeners and crosslinkers to be printable. [45]

In drug carrier research receptor binding peptides H2.1 and H2.2 were added to 15mer RSSP MS1 to aid in targeting cells overexpressing growth factor receptor Her2, which is typical for tumor tissue. The RSSP and binding peptides retained their functions, and the functionalized RSSP spheres were shown to target tumor cells, albeit with some unspecificity. The spheres were loaded with cancer drug (doxorubicin) and showed pH dependent release. [46] Jansson et al. added small affinity domains (6-17 kDa) for IgG (Z and C2), albumin (ABD) and biotin (M4) to 4RepCT RSSP. All domains showed affinity to their corresponding targets indicating proper folding and accessibility, and they did not hinder silk assembly progress. While the study was not related to biomedical science, it shows that it is possible to fuse RSSP with moderately sized protein domains without losing properties of the silk or the fused protein. [47]

In the present study three silk like fusion proteins based on native ADF3 were used; CBM-ADF3-CBM, CBM-ADF3-FB_H-Crys and Crys-ADF3-FB_H-Crys. The previous studies showed that it is possible to enhance biocompatibility of RSSP by introducing cell adhesion sites, and that small proteins (~20 kDa) can be added without hampering properties of the fused protein or RSSP. However, there has not been prior biomedical research on RSSP with native ADF3 or its analogue eADF3, and the heparin binding site has not been used with other than hES cells [26]. Biocompatibility and cytotoxicity of ADF3 and compatibility of the heparin binding site with human dermal fibroblasts are addressed in this study. Moreover this study presents preliminary results of humanization of silk protein with human proteins as terminal domains.

3 Materials and methods

Important methods and materials for the experimental part will be explained in this section in chronological order.

3.1 Spider silk constructs

Three different fusion proteins were used in the cell culture experiments (Figure 5): CBM-ADF3-CBM, CBM-ADF3-FB_H-Crys and Crys-ADF3-FB_H-Crys. The fusion proteins were designed by Sesilja Aranko, and the expression plasmids were assembled by Ellinor Englund. The central part was a major ampulla gland silk fibroin 3 (ADF3) from *Araneus diadematus* (Uniprot Q16987) without the terminal domains (43 kDa), which has been codon optimized for *E. coli*. The terminal constructs were cellulose binding module (CBM) (17.3 kDa) from *Ruminiclostridium thermocellum* and gamma crystallin D (Crys) (20.3 kDa) from *Homo sapiens*, and they were attached to ADF3 by linker peptides. The peptide sequence FB_H was a nine amino-acids long heparin binding site found in fibronectin (sequence GWQPPRARI). All fusion proteins contained a histidine tag (H_6) for affinity purification.

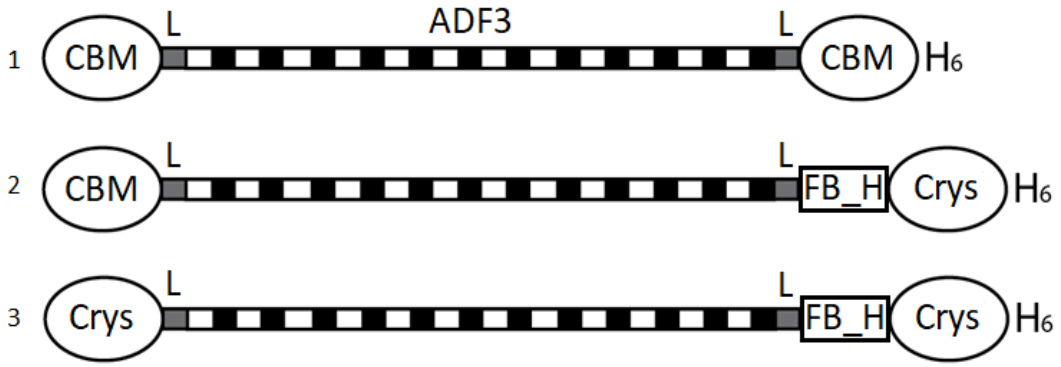

Figure 5. Silk like fusion proteins. ADF3 = native gland silk fibroin 3 from *Araneus diadematus* without terminal units. CBM = cellulose binding module from *Ruminiclostridium thermocellum*. Crys = gamma crystallin D from *Homo sapiens*. FB_H = heparin binding site from fibronectin. L = linker for terminal domains. H_6 = histidine tag. 1= CBM-ADF3-CBM, 2 = CBM-ADF3-FB_H-Crys, 3 = Crys-ADF3-FB_H-Crys.

3.2 ClearColi BL21, transformation and preparation of glycerol stocks

ClearColi BL21 (DE3) strain by Lucigen was used in production of the spider silk. The difference to normal *E. coli* BL21 (DE3) is that it has modified LPS, lipid IV_A, which does not contain oligosaccharide chains and has only four acyl chains instead of six (Figure 6). Removal of oligosaccharide chains makes it easier to remove the LPS in purification steps. Inflammatory effect of endotoxin comes from recognition

of the six acyl chains by Toll-like receptor 4 (TLR4), and with four acyl chains lipid IV_A does not trigger endotoxic response in mammalian cells. Thus, there is no need for extensive washing steps to remove endotoxin from the product or quantification of endotoxicity with LAL endotoxin assays. The downside is approximately 50 % slower growth rate of normal *E. coli* BL21 (DE3). [48]

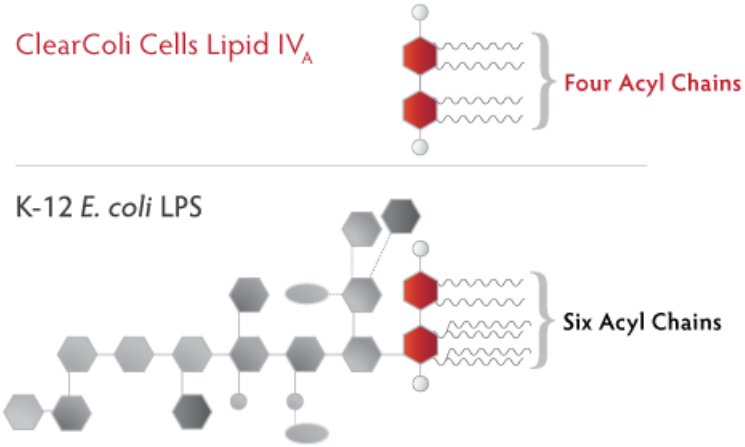

Figure 6. Lipopolysaccharide of ClearColi BL21 and normal *E. coli* BL21. Grey components are saccharides (O polysaccharide), red components are glucosamine residues flanked with phosphate groups (white sphere), and the chains are acyl chains. Modified from: [48].

Electrocompetent ClearColi BL21 (*E. coli*) cells were transformed with plasmids containing expression cassette for the previously mentioned silk constructs and antibiotic resistance for kanamycin according to Lucigen's transformation protocol. 25 µl of electrocompetent cells were thawed and pipetted to an ice-cold electroporation cuvette with 0.1 mm gap. 1 µl of around 10 ng/µl plasmid DNA was added, and it was mixed by flicking the cuvette. After a few minutes, the cells were electroporated with 1.8 kV (unknown capacity, and immediately 975 µl of Expression Recovery Medium at room temperature (RT) was added in the cuvette. The mixture was pipetted to a 10 ml culture tube, and incubated in 37 °C 200 rpm for 1 hour. 10-100 µl of the cell mixture was plated on a LB-Miller or LB-Lennox plate containing 50 µg/ml kanamycin, and incubated for 1-2 days in 37 °C. After overnight incubation the colonies were small with diameter less than 1 mm. There was no significant difference noticed in growth speed between LB-Miller and LB-Lennox. [48]

Preparation of glycerol stocks for long-term storage was initially done by inoculating 5 ml LB-Lennox (50 µg/ml kanamycin) with transformed ClearColi strain and incubated over 6 h in 37 °C 200 rpm, as suggested by Lucigen. 500 µl of the cell broth was mixed with 500 µl sterile 25 % glycerol and flash freezed with liquid nitrogen before storing in -80 °C. However, this was noted to result in poor stocks that were difficult to revive. With OD_{600} measurements it was apparent that

liquid cell culture inoculated from a plate had a long lag time (4-6 h) until proper growth. Thus, preculture (LB-Miller with 50 µg/ml kanamycin) was inoculated with a transformed colony and it was incubated overnight 37 °C 220 rpm. 500 µl of the preculture was moved to 5 ml LB-Miller with 50 µg/ml kanamycin, and incubated till OD 0.6-0.8 (~3-4 h), which was mixed with glycerol and stored as previously explained. [48]

3.3 Silk protein production with *E. coli*

Precultures were generally conducted by inoculating 100 ml LB containing 50 µg/ml kanamycin with ClearColi glycerol stock, and incubated overnight in 37 °C 220 rpm. Precultures were diluted in 1 L of LB with kanamycin resulting in 0.1 OD_{600}. In the first four production batches cultures were incubated in 37 °C 220 rpm for 24 h, and LB-Lennox was used as a media. In the following batch incubation time was reduced to 2-3 h for the culture to reach 0.6-0.8 OD, and media was changed to LB-Miller, which increased product yields significantly. Cultures were induced with 0.2 mM IPTG, and incubated in 30 °C 220 rpm for 24 h.

The cells were harvested by centrifuging 18700 rcf 20 min RT, and lysed by incubating in 100 ml lysis buffer (50 mM TRIS-HCL pH 7.4, 3 mM $MgCl_2$, DNase-A, lysozyme, 1 tablet of SigmaFast protease inhibitor cocktail) / 2 L culture for 40 minutes 200 rpm in RT. The cells were erupted with EmulsiFlex C3 homogenizer. Soluble silk protein was harvested by centrifuging 25000 rcf for 2 h in RT and collecting the supernatant. Supernatant was flash freezed with liquid nitrogen and stored in -80 °C.

3.4 Fast protein liquid chromatography

The silk proteins were separated from the lysis supernatant with fast protein liquid chromatography (FPLC) (ÄKTA pure by GE Healthcare), which separates components according to their affinity to the column material. Silk protein constructs contained His-tags, which have high affinity to nickel. During FPLC the lysis supernatant was injected in the nickel column that binds to proteins with His-tag. The column was washed with buffer solution to remove impurities that had low affinity to nickel. The column was eluted with gradually increasing concentration of imidazole, which at certain point released the His-tag protein due to imidazole's higher affinity to nickel. Elution of proteins were seen as a spike in UV 280 nm detector located in downstream.

Three 5 ml His-Tag columns were used, and 100 ml of supernatant was loaded per one run. Binding buffer was 20 mM imidazole, 500 mM NaCl, pH 7.4, and elution buffer 500 mM imidazole, 500 mM NaCl, pH 7.4. Phosphate was not added in the buffers as it was noticed to aggregate silk proteins. Eluted products were flash freezed with liquid nitrogen and stored in -80 °C.

3.5 Concentration and washing of silk protein

The eluted silk protein solution were initially washed from imidazole, salt and other impurities with Econo-Pac gravity-flow chromatography column by adding 3 ml lysis supernatant and then 5 ml TRIS-HCl while collecting the flow-through. However, due to the loss of product and significant time investment, this washing step was only done with the first two silk protein batches.

Concentration and additional washing was done with 20 ml Vivaspin 30 kDa protein concentrator spin columns. Each sample (10-50 ml) was concentrated to volume of 5 ml by centrifuging 3500 rcf 30 °C. The concentrate was washed three times with 15 ml sterile 50 mM TRIS-HCl pH 7.4, and concentrated to volume of 0.5-1.5 ml, both with the previous centrifuge settings. The final concentrate was filtered with 0.20 µm filter, and the protein concentration was measured with Nanodrop.

3.6 SDS-PAGE

SDS-PAGE was used to detect the presence of the silk constructs and estimate the amount other protein contaminants or degraded silk proteins in the silk concentrates. The separation and stacking gel were done according to Table 2 with 9 and 5 % acrylamide content, respectively. Both gel solutions were incubated for 40 minutes RT. Protein samples were denatured and dyed by using 4X loading dye with DTT and incubating for 5 minutes in 92 °C. Generally 20 µl of 2 mg/ml denatured protein solution was added in the wells. 5 µl of Bio-Rad's Precision Plus Protein Dual Color Standard (10-250 kDa) was used as the ladder, and the gel was ran with 80V until proteins passed the stacking gel and then the voltage was increased to 100V. The gel was stained with Coomassie Blue for overnight and destained with destaining solution (42.5 % ethanol, 10 % acetic acid) for 2 hours, both in RT with 180 rpm shaking. Imaging was done with Gel Doc XR (BioRad).

Table 2. Preparation of gel solutions for SDS-PAGE.

	Separating gel	Stacking gel
H2O	3,19 ml	2.57 ml
TRIS-HCl	2.25 ml (1.5 M, pH 8.8)	437 µl (1 M, pH 6.8)
APS	95.14 µl	33,3 µl
SDS (10 %)	95.14 µl	33,3 µl
TEMED	3.71 µl	3,3 µl
Acrylamide (40 %)	2,25 ml	437 µl

3.7 Production of silk films

Two methods were used to form spider silk films. In the first method liquid silk concentrate was spread evenly on a glass coverslip, and it was incubated in RT until the liquid was completely evaporated, generally overnight, in sterile conditions. 100-150 µl of 2-3 mg/ml silk concentrate was added on a glass slide with diameter of 22 mm, resulting in around 0.08 mg/cm^2.

When moving to smaller sample areas such as 96-well plates, more convenient method was required. Thus, 50-100 µl of 0.3 mg/ml silk concentrate was added per well and incubated 2 h RT. The remaining solution was aspirated and the plate was incubated overnight RT in laminar. Similar method was used by Widhe et al. in "A fibronectin mimetic motif improves integrin mediated cell biding to recombinant spider silk matrices". [13]

3.8 Fibroblast cell culturing

Human dermal fibroblast (HDF) isolated from adult skin (Gibco™ C0135C) was used for the cytotoxicity and biocompatibility tests. HDF is a robust and adherent cell type that is found in dermis of skin embedded in ECM. It is a dynamic cell lineage capable of changing its phenotype according to different stimuli from ECM, and the presence of surface that it can adhere onto is necessary for its survival. Thus, HDF is suitable for the preliminary tests. It can also be induced into a pluripotent stem cell line for further research. HDFs can produce ECM components to its local surroundings, and it is the main producer of ECM components in healing wounds. [49] Thus, it is possible that it can alter its surroundings even in the test conditions giving better results for the scaffold materials.

Mammalian cultures are susceptible to many contaminations due to their slow growth, favorable media and lack of antibiotics, and thus good aseptic technique was essential part of cultivating fibroblasts. The cultures were always handled in Class II Biological Safety Cabinet with HEPA filtered laminar airflow dedicated purely to mammalian cells. Tools were sterilized with 70 % ethanol before moving them to the laminar, and only sterile reagents were used. Gloves and clean laboratory coat were always worn.

Normal culturing of HDF was done in a plastic petri dish coated with gelatin. 10 ml of sterile 0.1 % gelatin was added in a petri dish, and incubated for 20 min in RT. The remaining solution was aspirated and the dish was dried for 10 min. 20 ml of HDF growth media (Cell Applications, Inc.) at 37 °C was pipetted in the dish. The dish was seeded with 10^5-10^6 fibroblasts from a cryostock or trypsinated cells from previous culture. If cryostock was used, it was thawed in water bath 37 °C until a small bit of ice was left and then promptly pipetted in the dish. With trypsinated cells around 0.5-2.0 ml of the cell mixture was used for seeding. The petri dish was

mixed by swirling gently to spread the cells evenly and then moved in a CO_2 incubator (37 °C, 5 % CO_2). The media was changed daily by aspirating old media and adding 20 ml of fresh HDF growth media (37 °C) slowly to the side of the dish. In some cases 100X antibiotic cocktail containing 10000 U/ml penicillin and 10000 µg/ml streptomycin was used by adding 10 µl cocktail per 1 ml of media. Continuous usage of antibiotic is not recommended as it masks poor aseptic technique and thus potentially exposing the culture to other contaminations, such as yeast, mycoplasma and antibiotic resistant bacteria.

Subculturing and preparation of cryostocks were done according to the provider's (Sigma-Aldrich) protocol [50]. The culture was grown to 70-90 % confluency, taking typically 3-5 days. The dish was washed with sterile PBS (37 °C) to remove cell clumps and trypsin inhibiting media. 3 ml of Trypsin-EDTA was added, and the dish was incubated up to 5 minutes while rocking and hitting the side of it every one minute to assist in releasing the bound cells. During incubation the dish was inspected with microscope to see if the cells had turned into spheres, indicating successful trypsination. Trypsin was inhibited by adding 6 ml Dulbecco's Modified Eagle Medium (DMEM), and the solution was collected to a Falcon tube. The dish was washed with 5 ml of DMEM, and pipetted to the Falcon tube to collect the remaining cells. Inhibition of trypsin should not be delayed as it damages the cells due to its proteolytic activity. The cell density of the cell mixture was analyzed with Countess II FL Automated Cell Counter by Invitrogen. For subculturing, the cell mixture was used for the seeding. For cryostock preparation, the cell mixture was centrifuged 220 rcf 4 °C for 5 minutes. The supernatant was aspirated and the cell pellet was resuspended in Recovery Freezing Medium by Gibco containing 10 % dimethyl sulfoxide (DMSO), and pipetted in 0.5-1 ml aliquots to cryovials. The cryovials were frozen with controlled rate (~1 °C/min) by placing them in an isopropanol bath, which was stored in -20 °C for 2 hours and then moved to -80 °C for overnight. For long term storage the cryovials were moved to -150 °C without the isopropanol bath. During preparation and revival of cryostocks the cells are exposed to DMSO, which makes the cell membrane porous protecting it from thawing, but it is also detrimental to the viability of the cell [51]. This was noticed during the experiments; with prolonged preparation the fibroblast cryostocks were unable to revive, which was prevented by minimizing the exposure time from over 1 hour to 10 minutes.

3.9 Microscopy

Leica microscope with 10X lens was used to examine fibroblast cultures; e.g. possible contaminations, estimate confluency and recognize dead or unattached cells. The microscope was not used to create statistically good quantitative data about amount of cells or viability, as it was too time consuming to get a sufficient representative of each sample. The microscope also included a camera (Leica DFC

3000 G with software Leica LAS X) and a fluorescence illuminator (Leica CoolLED's pE-300^{white}).

3.10 DAPI staining

To ease the counting of the cells, DAPI (4,6-Diamidino-2-Phenylindole) was used to stain the nuclei of the cells. After cultivation of the sample, e.g. a seeded well in 12-well plate, it was washed three times with PBS (37 °C) and the cells were fixated with 8 minute incubation in 4 % polyformaldehyde (PFA) in PBS at RT. The washing step (3x) was repeated and the cells were permeabilized with 8 minute incubation in 0.1 % Triton X-100 in PBS at RT, and washed three times. The cells were stained with 1 µg/ml DAPI in PBS for 5 minutes at RT in dark, and washed twice. The samples were then imaged with fluorescence camera with 400 nm excitation and 460 nm emission. Without fixation and permeabilization DAPI staining of live cells was noted to be very poor. Initially it was planned that the fluorescence would be measured with a plate reader (Cytation 3 BioTek), and then compare the results between the samples. However, the readings were close to zero in all samples.

3.11 Cell viability analysis with MTT

In most cells mitochondrial activity is associated with cell viability, and thus NADH level can be used to roughly estimate cell viability. MTT (3-(4,5-dimethylthiazol-2-yl)-2,5-diphenyltetrazolium bromide) oxidizes NADH inside the cells forming purple formazan, which can be dissolved and measured with absorbance at 540 and 720 nm. Unlike staining and counting the cells, MTT gives more homogenous measurement resulting in better quantitative data about cell viability. [52]

MTT assay was performed with 96-well plates that were coated with different scaffold materials as explained in 3.2.5. The plate was seeded with 100 µl/well of HDF media containing 10^5-10^6 trypsinated fibroblasts/ml. The plate contained control wells (bovine serum albumin (BSA), gelatin) and blank wells (without cells). Minimum of three technical replicates were used for each scaffold material and each set of samples were seeded with the same amount of cells to keep the results comparable. The plate was incubated in a CO_2 incubator (37 °C, 5 % CO_2) for 1-2 days and the media was changed daily. For estimating the cell viability 10 µl of 5 mg/ml MTT in PBS was added to one set of samples and incubated for 4 hours in a CO_2 incubator. The media was aspirated and the formazan crystal were dissolved by adding 100 µl DMSO/well and incubating for 5 minutes in RT inside aluminum foil. The plate was read with an Eon BioTek plate reader by setting the protocol to 567 cpm (3 mm) linear shake for 1 minute, 10 second delay and measure absorbance at 570 nm. 570 nm was used instead of 540 nm due to more repeatable measurements. If the plate contained multiple sample sets, the DMSO was removed

and the plate was put back to the CO_2 incubator. All pipetting was done with a multichannel pipette to reduce variability due to pipetting errors.

3.12 Cell adhesion assay

In addition to cell viability, cell adhesion plays important part in evaluation of scaffold material biocompatibility. The assay was done in 96-well plates that were coated with scaffold materials as explained in 3.2.5, with control wells (gelatin, BSA) and blank wells (without cells). The wells were seeded with 100 µl HDF media containing $1x10^6$ trypsinated fibroblasts / ml and incubated in a CO_2 incubator (37 °C, 5 % CO_2) for 3 hours. The wells were washed three times with PBS (37 °C) to remove unattached cells. The cells were fixed by incubating in 4 % PFA for 8 minutes at RT, and washed once with PBS. The staining was done with Crystal Violet by pipetting 70 µl/well of 0.5 % Crystal Violet in 25 % methanol and incubating for 10 minutes at RT. Crystal Violet was washed with tap water by gently pouring it over the plate. The plate was turned upside down and dried for 1 hour at RT with vacuum evaporation. Crystal Violet was dissolved by incubating with 200 µl methanol per well for 30 minutes at RT, and the absorbance was measured at 570 nm with an Eon BioTek plate reader. Protocol for the measurement was set to 567 cpm (3 mm) linear shake for 1 minute, 10 second delay and measure absorbance at 570 nm.

3.13 Structural analysis of silk films

Measurement of contact angle and Fourier-transform infrared spectroscopy (FTIR) were used for structural analysis of the silk films. The silk films for contact angle measurement were prepared on clear polystyrene surface (downside of 96-well plate and upside of a petri dish lid) by adding 50 µl of 0.3 mg/ml protein solution and letting it incubate for 2 hours at RT with or without cover. Without cover the solution evaporated completely resembling the method 1 in 3.7. After incubation with a cover, the remaining solution was aspirated to mimic coating in method 2. In both methods the films were kept in laminar for overnight at RT. The measurements were done with Attension Theta (Biolin Scientific). The injected amount of deionized water varied from 0.5 to 2.0 µl. In cases where the droplet formed an asymmetrical shape, a new droplet was injected, since the angle was not uniform at all sides.

FTIR detects molecular vibrations of stretching and bending chemical bonds. The resulting data can be used to determine the structure of the sample; e.g. C=O stretching coupled with in-plane N-H bending can be seen as a strong peak in region 1600-1700 cm^{-1}. This is called amide I band in protein IR, and the exact location of the peak changes when it originates from α-helices or β-sheets. Thus, the location of the amide I can be used to draw conclusions about the secondary structure of the protein. Other structural sensitive bands are amide II-VII. However, quantitative

estimation of secondary structure is often not trivial and requires additional tools such as pattern recognition algorithms for the results to be reliable. Also, the peak location for a certain secondary structure, such as α-helix, is not necessary the same for different proteins, thus making comparison of secondary structure difficult. [53] Here the IR spectra was only used to draw conclusion about the structural differences between silk fusion proteins without specifying where it originates from. IR measurement of silk films was done with PerkinElmer Spectrum 2 FT-IR Spectrometer by adding 5 µl of 5 mg/ml protein solution on the diamond lens and evaporating it for at least 40 minutes. The IR spectra was normalized with Spectrum software by dividing each absorbance value with the highest peak absorbance.

3.14 Scanning electron microscope

Scanning electron microscope was used briefly to image the cells adhering to the silk films for qualitative data, but due to rough sample preparation all of the cells had been disrupted. The HDF cultures on glass slides were washed with PBS and fixed with increasing gradient of formaldehyde (FA) from 4 to 10 % in steps of 2 with 10 minute incubation at RT. It should be noted that the FA (formalin) contained around 10 % methanol to prevent the polymerization of the FA. Methanol dehydrates the cells rapidly which can affect the morphology of the cell by shrinking it. The samples were stored in 4 % FA at 4 °C. Prior to SEM imaging, the samples were doused in liquid nitrogen and dried in vacuum evaporator for overnight. The samples were sputtered with platinum and imaged with SEM.

With the previous protocol the cells were disrupted and thus a gentler sample preparation was needed. In SEM sample preparation aimed for biological samples the cell samples on glass slides were washed with PBS (37 °C) and fixed with 2.5 % glutaraldehyde in PBS for 30 minutes at RT. The samples were then dehydrated by adding an increasing alcohol gradient using 25, 40, 60, 80, 90 and 100 % ethanol, each step with 15 minute incubation at RT. Ethanol was evaporated by using a desiccator for minimum of 30 minutes. [54] However, the samples were not imaged due to lack of time. The assumption is that this method would be more suitable for delicate cell samples.

3.15 Statistics

One-way analysis of variance (ANOVA) was used to compare expected values of the sample groups and find significant differences. The null hypothesis (H_0) of ANOVA is that all samples come from the same distribution. Assumptions are that the samples are independent and identically distributed (IID), the variances of the populations are equal and the residuals are normally distributed. Violation of these assumptions leads to unreliable results; especially IID and homogeneity of population variances are crucial for ANOVA to work properly. ANOVA produces F-statistics, which is used to determine if H_0 is rejected. Here significance level (α)

0.05 was used. If p-value for F-statistics falls below α, H_0 is rejected. In such cases Tukey's Post Hoc Test was used to find significant difference between individual sample groups. It compares expected values between all sample pairs with H_0 that they come from the same distribution, and performs p-value correction so that the probability of rejecting one or more true H_0 is less than α for all comparisons. Tukey's test has the same assumptions as ANOVA. Assumptions about normality and equality of variances were tested with Shapiro-Wilk's and Bartlett's test, respectively ($\alpha = 0.05$). If equality of variances did not hold, Welch's t-test with Bonferroni's p-value adjustment was applied instead of ANOVA / Tukey. However, with low sample size the power of these statistical analyses is poor, and the results should be considered with caution. In some cases unequal sample sizes were used, which is not beneficial for statistical analyses as the power is determined by the lowest sample size.

Bar plots were used for graphical visualization with error bars set to be plus/minus the standard deviation (SD) indicating the spread of the data. When assuming normality, the error bar estimates the location of 66 % of the population. Standard deviation was chosen instead of standard error, which shows the accuracy of the calculated mean, because variance is also an important result together with the mean.

All data analysis was done with R programming language by using open source software RStudio.

4 Results

4.1 Production of silk like fusion proteins

The silk constructs were produced in five batches with varying results. The yields from 1 liter of culture are shown in Figure 7, and comparison of product quality between batch 4 and 5 after FPLC purification in Figure 8. The expected size of CBM-ADF3-CBM, CBM-ADF3-FB_H-Crys and Crys-ADF3-FB_H-Crys were 85 kDa, 85-88 kDa and 88 kDa, respectively. Thus, the wide bands in the protein gel were in the right locations. The smaller bands were assumed to be truncated silk proteins as they remained after FPLC purification. The production was optimized between batches 4 and, which could be seen in both yield and quality of the silk proteins.

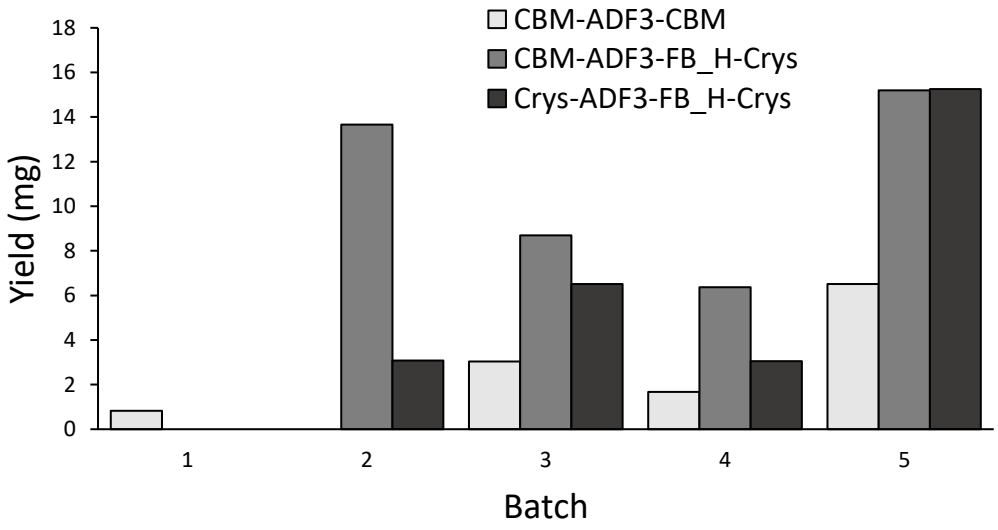

Figure 7. Yield (mg) of silk constructs from 1 L of cell culture (ClearColi BL21). The protocol was changed between batch 4 and 5, which can be seen in yield improvement.

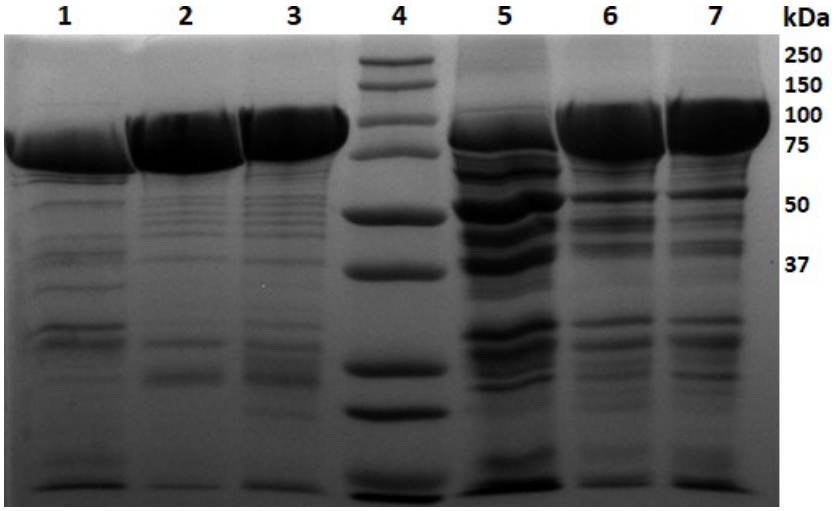

Figure 8. SDS-PAGE: Comparison of product quality between batch 5 (left) and 4 (right) after FPLC purification. 1 and 5 = CBM-ADF3-CBM. 2 and 6 = CBM-ADF3-FB_H-Crys. 3 and 7 = Crys-ADF3-FB_H-Crys. 4 = ladder. Expected sizes for complete silk constructs 85-88 kDa. Other bands are assumed to be truncated silk constructs.

4.2 Initial evaluation of cytotoxicity

Evaluation of cytotoxicity of the silk constructs was done with 12-well cultivations and coated glass slides as explained in chapters 3.7 and 3.8. In the first experiment majority of the wells were contaminated on day 1, including wells with uncoated glass slides. Initially no antibiotic was used, but addition of streptomycin and penicillin cocktail did not seem to be effective, thus indicating antibiotic resistance. The unknown organism had bacillus like shape and was often in diplobacilli form resembling *E. coli*, which would not be surprising as antibiotic resistant *E. coli* strains were commonly used in the laboratory. It was concluded that the contamination originated from non-sterile glass slides, and thus in the next experiments the glass slides were dry sterilized in 160 °C for minimum of 2 hours. The cell cultures were imaged with SEM for qualitative data and some of the images can be found in attachments (Attachment 1, Attachment 2 and Attachment 3). However, all of the cells were exploded indicating too harsh preparation method. The protocol for fixation and evaporation were changed to be more suitable for biological samples. In the second cytotoxicity experiment the HDF cryostocks did not revive. This was caused by incorrect preparation of the cryostocks that resulted in prolonged exposure of cells to DMSO. DMSO is used in cryopreservation but it is also toxic to cells at high concentrations [51]. The preparation method was changed to minimize the exposure time, which solved the problem.

The third experiment was successful. During seven-day cultivation there was no notable difference in growth between the silk films, uncoated glass (control), BSA and conventional matrix material gelatin. Images from 5th day of cultivation with

10X microscope before and after DAPI staining are presented in Figure 9, Figure 10, Figure 11, Figure 12 and Figure 13. Multiple images were taken from each sample, but only representative images are shown here. CMB-ADF3-FB_H-Crys and Crys-ADF3-FB_H-Crys contained notable amount of aggregates.

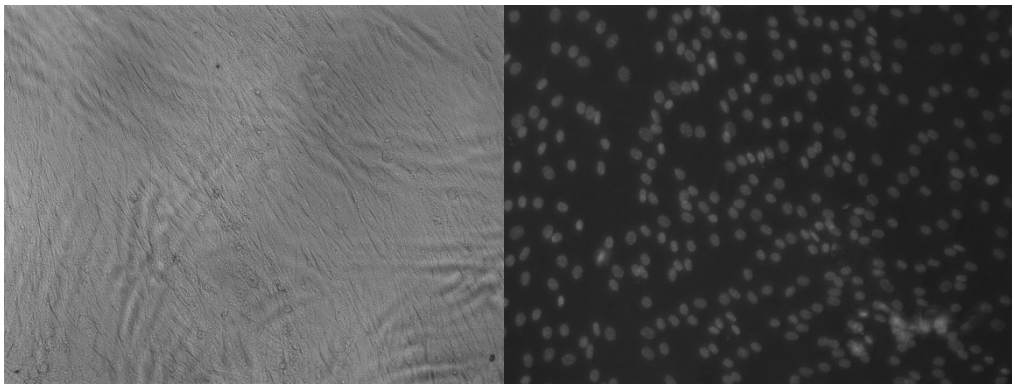

Figure 9. Evaluation of cytotoxicity: Fibroblast culture on glass surface after 5 days of incubation with (left) and without (right) DAPI staining.

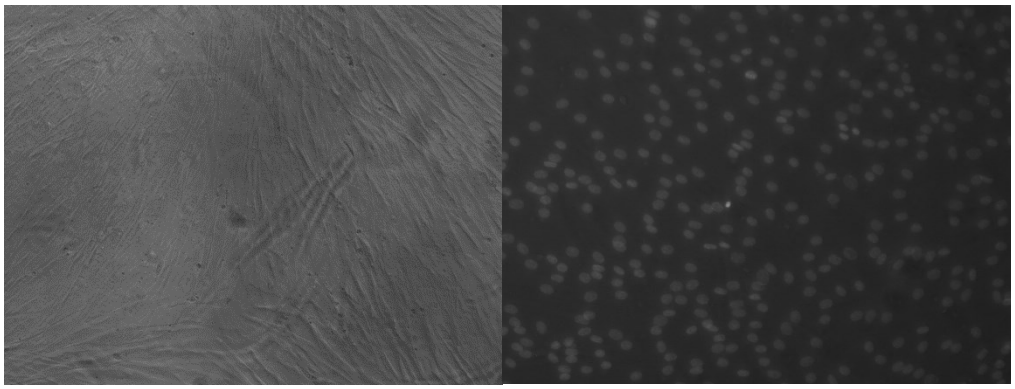

Figure 10. Evaluation of cytotoxicity: Fibroblast culture on gelatin film after 5 days of incubation with (left) and without (right) DAPI staining.

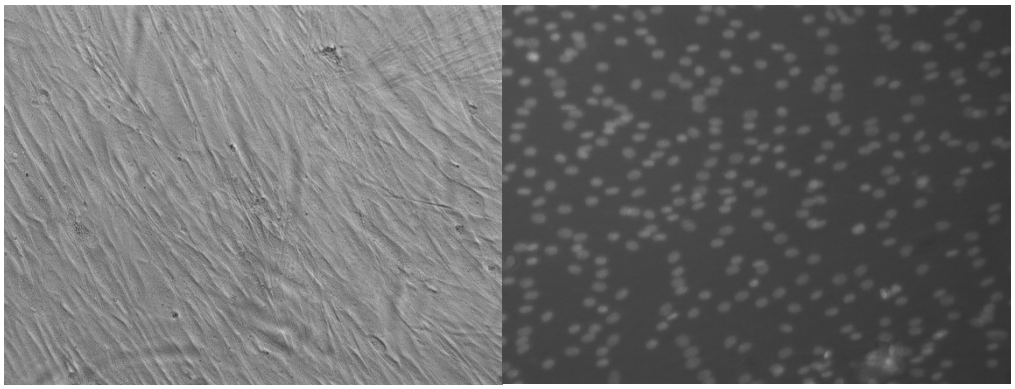

Figure 11. Evaluation of cytotoxicity: Fibroblast culture on CBM-ADF3-CBM film after 5 days of incubation with (left) and without (right) DAPI staining.

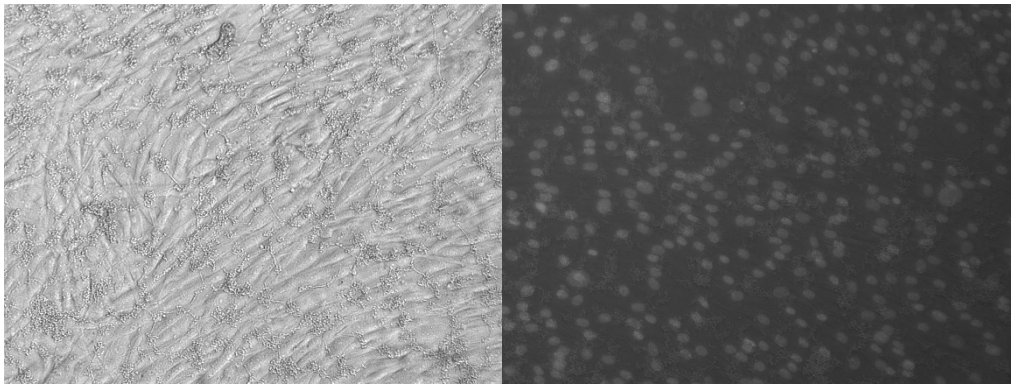

Figure 12. Evaluation of cytotoxicity: Fibroblast culture on CBM-ADF3-FB_H-Crys film after 5 days of incubation with (left) and without (right) DAPI staining.

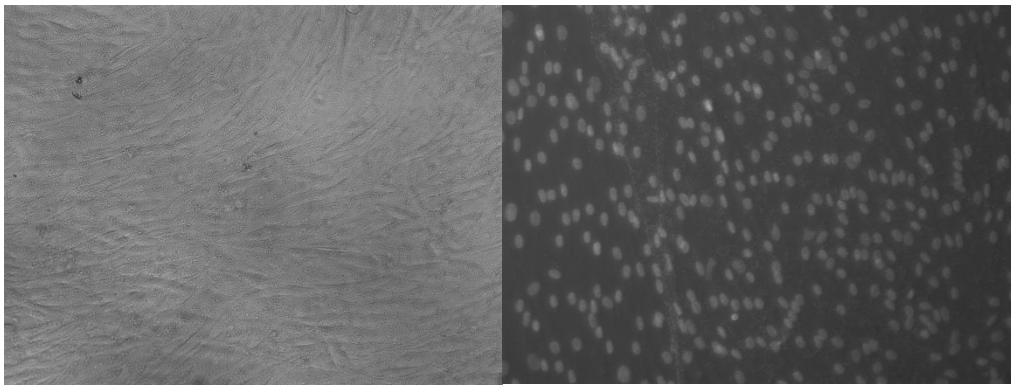

Figure 13. Evaluation of cytotoxicity: Fibroblast culture on Crys-ADF3-FB_H-Crys film after 5 days of incubation with (left) and without (right) DAPI staining.

4.3 Cell viability

The initial idea was to estimate cell viability by counting the amount of cells daily in cultivations with coated glass slides (12-well). However, it was quickly noted from the cytotoxicity tests that the cell density was not uniform and the results from cell counting differed considerably between different locations on the same sample. For meaningful quantitative results, there should have been multiple cell counts from each sample on daily basis, and with three technical replicates of six sample types this was not reasonable. DAPI staining was tested for automated cell counting but the plate reader (Cytation 3 BioTek) did not recognize the fluorescence of DAPI. It is possible that the settings given for the instrument were wrong or the placement of the sample was off due to unusual height. To solve this the optimal excitation and emission of DAPI could have been verified and optimized with fluorescence spectra analyzer and glass slides measured individually without the 12-well plate. However, it was noted by our colleague that the fluorescence measurement is taken from a single point, and scanning of larger area could not be implemented. Thus, homogeneous measurement was not possible to achieve with this method.

MTT was chosen for more convenient method for estimating the cell viability. It measures the concentration of NADH in the cells, which is an indication of mitochondrial activity [52]. Three MTT tests were conducted. In the first test too low amount of cells were seeded due to insufficient knowledge and error in calculations or in cell counter. The aimed seeding level was 500 cells / well. However, there were maximum of 20 cells / well (96-well plate), and they divided very slowly in all of the samples. The MTT results from 5 days old cultures did not differ between blanks and samples. The test was repeated with higher seeding amount, and two seeding levels were tested; 10 000 and 50 000 cells/well with three technical replicates. The results are shown in Figure 14 and Figure 15 for day 1, and Figure 16 and Figure 17 for day 2 measurements.

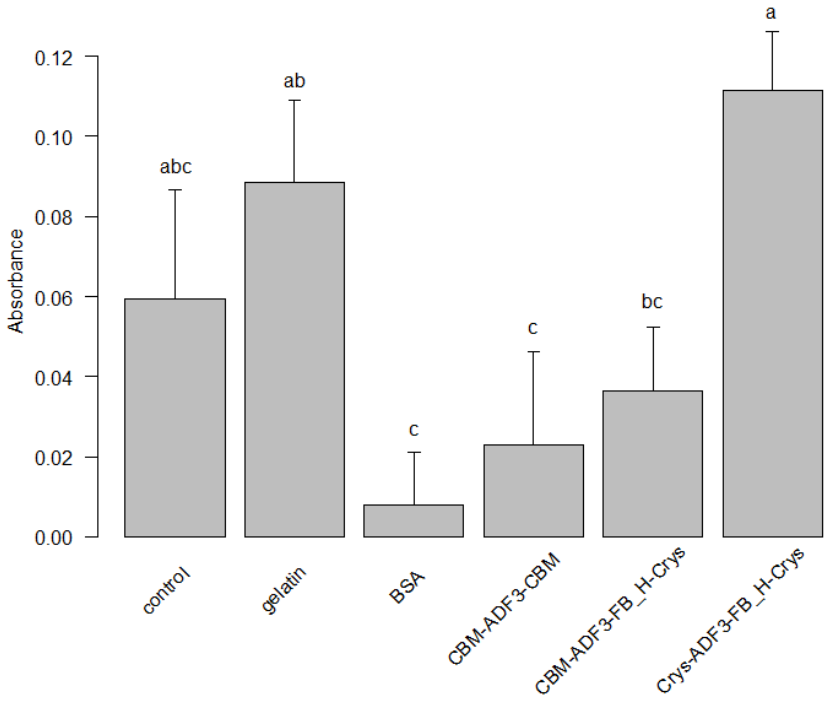

Figure 14. MTT (cell viability assay) test 2 on day 1 with low cell seeding (10 000 cells/well). Control is from uncoated wells. Gelatin and BSA are used as conventional materials. Significance levels are denoted with different letters (a, b, c) on top of error bars. Letters shared in common between samples indicate no significant difference (ANOVA/Tukey Post Hoc, p-value < 0.05). Error bar ± 1 SD. Sample size 3.

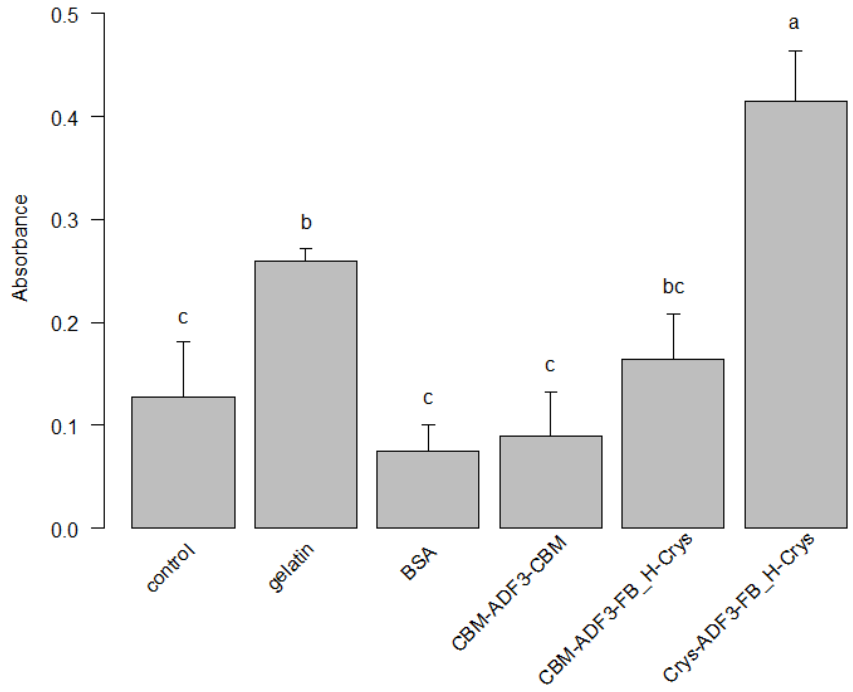

Figure 15. MTT (cell viability assay) test 2 on day 1 with high cell seeding (50 000 cells/well). Control is from uncoated wells. Gelatin and BSA are used as conventional materials. Significance levels are denoted with different letters (a, b, c) on top of error bars. Letters shared in common between samples indicate no significant difference (ANOVA/Tukey Post Hoc, p-value < 0.05). Error bar ± 1 SD. Sample size 3.

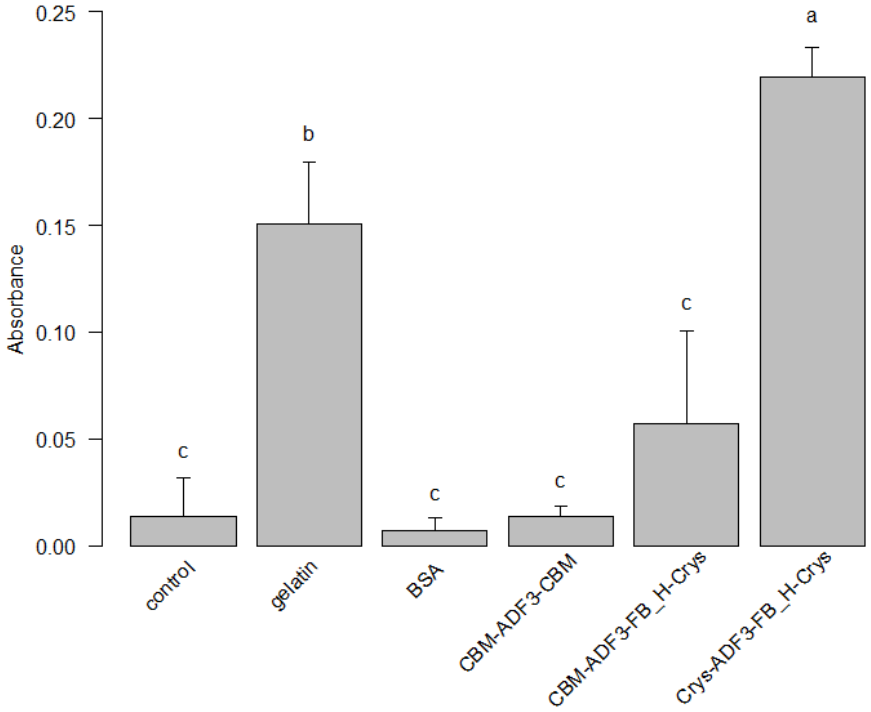

Figure 16. MTT (cell viability assay) test 2 on day 2 with low cell seeding (10 000 cells/well). Control is from uncoated wells. Gelatin and BSA are used as conventional materials. Significance levels are denoted with different letters (a, b, c) on top of error bars. Letters shared in common between samples indicate no significant difference (ANOVA/Tukey Post Hoc, p-value < 0.05). Error bar ± 1 SD. Sample size 3.

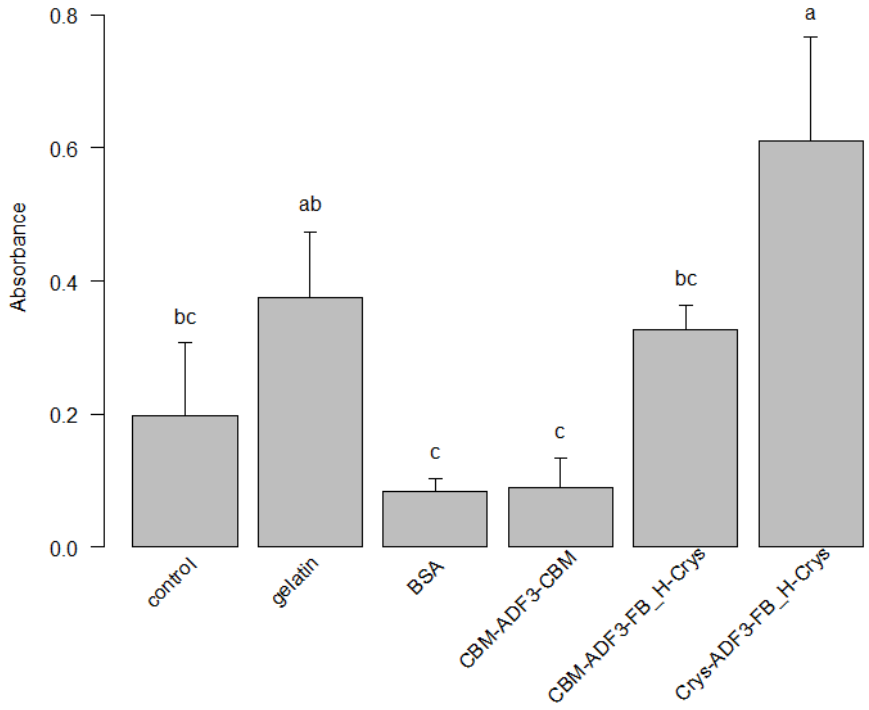

Figure 17. MTT (cell viability assay) test 2 on day 2 with high cell seeding (50 000 cells/well). Control is from uncoated wells. Gelatin and BSA are used as conventional materials. Significance levels are denoted with different letters (a, b, c) on top of error bars. Letters shared in common between samples indicate no significant difference (ANOVA/Tukey Post Hoc, p-value < 0.05). Error bar ± 1 SD. Sample size 3.

MTT test was repeated to verify that the results were repeatable. In the third test 40 000 cells were seeded per well and the sample size was increased to 6 for control, BSA and gelatin, and 8 for silk constructs (Figure 18 and Figure 19). While the results had the same trend as in the previous test, the absorbance level was same for day 1 and 2 measurements, and BSA and CBM-ADF3-CBM gave negative absorbance on day 2 indicating total loss of cells. This could be caused by the 1 minute shaking (567 cpm) during day 1 measurement as all the samples were on the same 96-well plate.

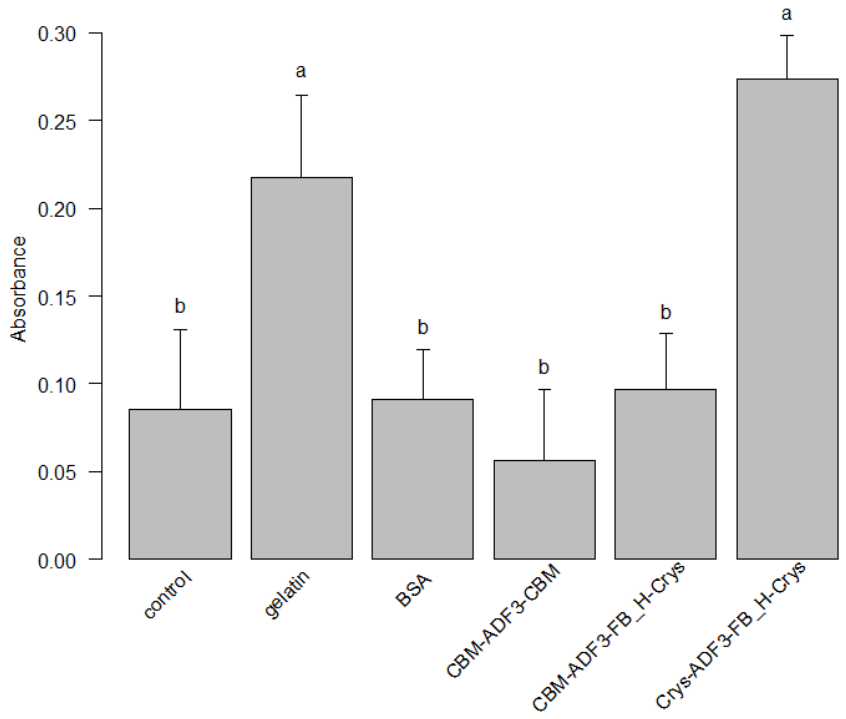

Figure 18. MTT (cell viability assay) test 3 on day 1. Control is from uncoated wells. Gelatin and BSA are used as conventional materials. Significance levels are denoted with different letters (a, b, c) on top of error bars. Letters shared in common between samples indicate no significant difference (ANOVA/Tukey Post Hoc, p-value < 0.05). Error bar ± 1 SD. Sample size 6 for control, gelatin, BSA, and 8 for silk constructs.

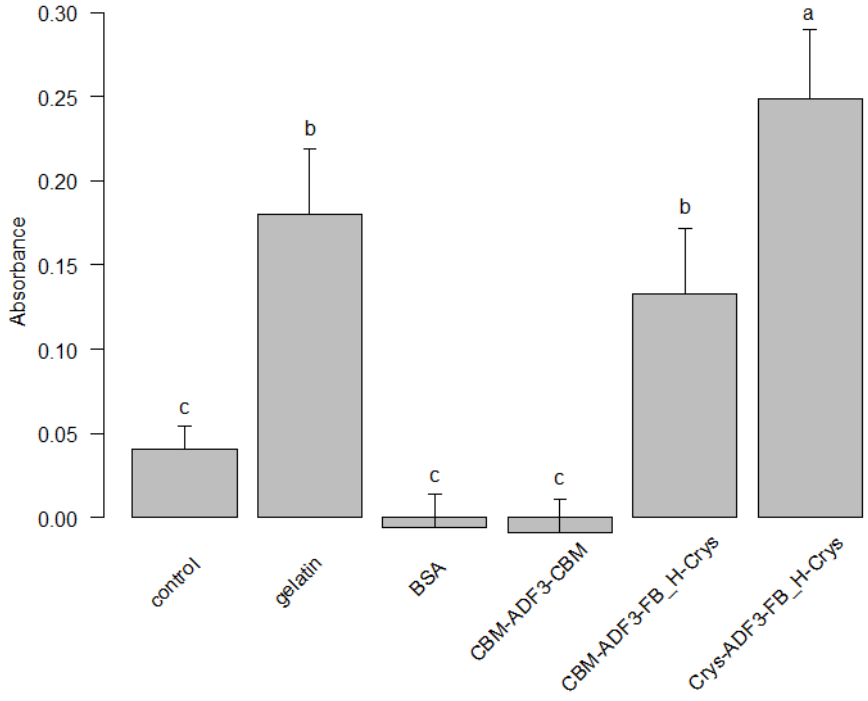

Figure 19. MTT (cell viability assay) test 3 on day 2. Control is from uncoated wells. Gelatin and BSA are used as conventional materials. Significance levels are denoted with different letters (a, b, c) on top of error bars. Letters shared in common between samples indicate no significant difference (ANOVA/Tukey Post Hoc, p-value < 0.05). Error bar ± 1 SD. Sample size 6 for control, gelatin, BSA, and 8 for silk constructs.

4.4 Cell adhesion

Cell adhesion on the silk constructs was tested with adhesion assay. In the first test around 100 000 cells were seeded per well (Figure 20). The actual amount was unknown due to unreliable measurement by the cell counter, but assumedly the concentration was much higher than displayed by the cell counter. The experiment was repeated with lower cell density (70 000 cells/well) to verify repeatability (Figure 21). The samples had very different variances, which in result led to low probability of equal population variances. Thus, Welch's t-test with p-value adjustment was used instead of ANOVA / Post Hoc Tukey's test. CBM-ADF3-FB_H-Crys in test 2 had many outliers lowering the probability of coming from normal distribution below 5 % preventing from using conventional statistical analysis methods. While variety in variances could be a meaningful result, here the cause was most likely non-systematic washing step for removing excess Crystal Violet from the samples.

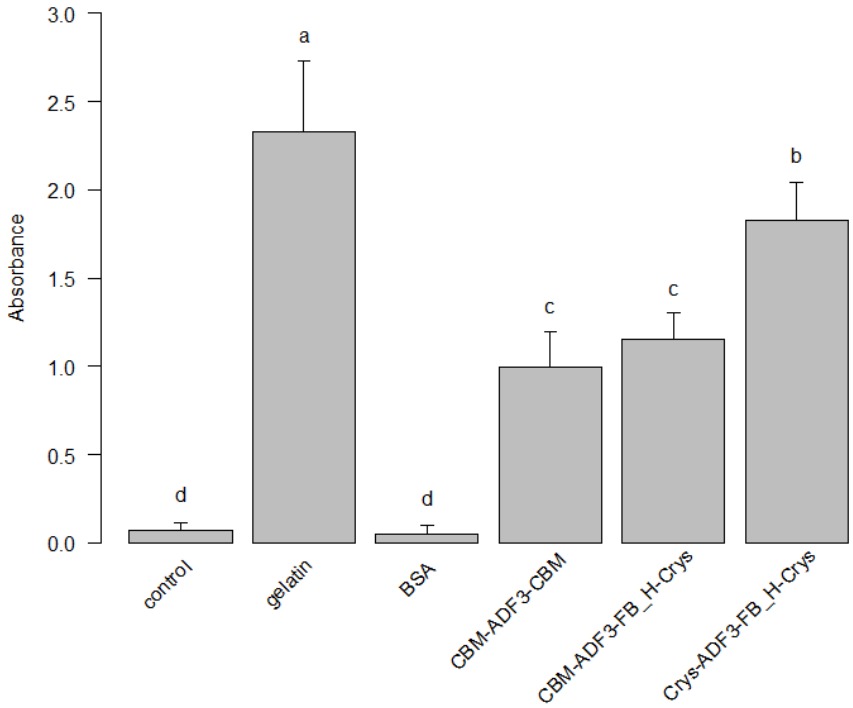

Figure 20. Cell adhesion test 1 Control is uncoated well. Gelatin and BSA are conventional materials. Significance levels are denoted with different letters (a, b, c, d) on top of error bars. Letters shared in common between samples indicate no significant difference (Welch's t-test and Bonferroni p-value adjustment, p-value < 0.05). Error bar ± 1 SD. Sample size 12 for control and gelatin, and 16 for BSA and silk constructs.

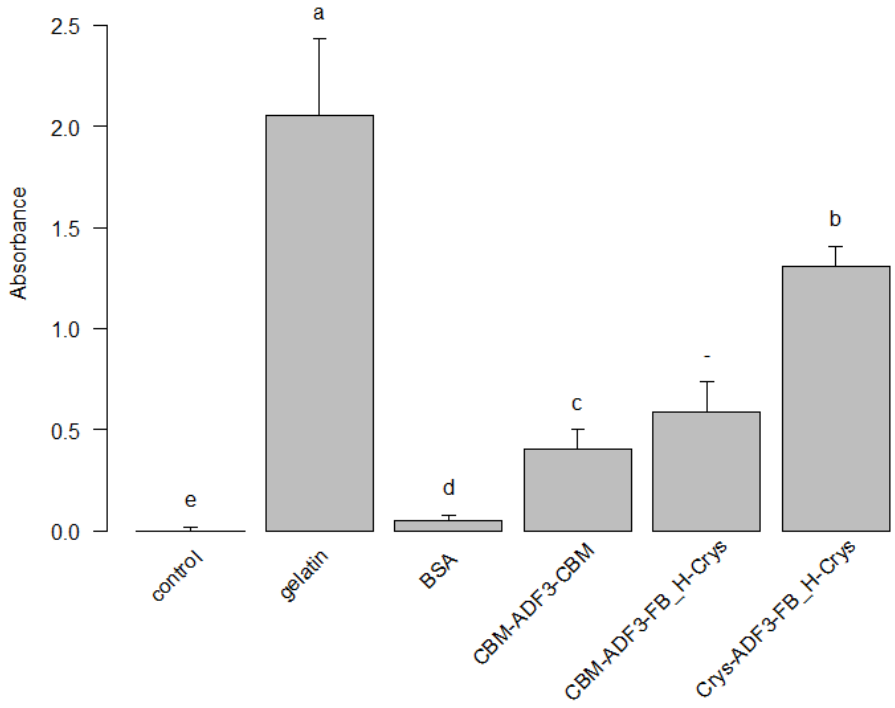

Figure 21. Cell adhesion test 2. Control is uncoated well. Gelatin and BSA are conventional materials. Significance levels are denoted with different letters (a, b, c, d) on top of error bars. Letters shared in common between samples indicate no significant difference (Welch's t-test and Bonferroni p-value adjustment, p-value < 0.05). CBM-ADF3-FB_H-Crys unlikely to be from normal distribution. Error bar ± 1 SD. Sample size 14.

4.5 Structural analysis of silk films

4.5.1 Contact angle

Contact angle (CA) measurements were done to get some idea about the surface properties of the silk films, and possibly make a rough comparison about the amount of protein in the films according to hydrophilicity. The silk and control films were prepared on downside of 96-well plate by adding 50 µl 0.3 mg/ml protein solution and incubating it overnight at RT. The CA measurements are shown in Figure 22. Controls and CBM-ADF3-CBM showed expected behavior, but CBM-ADF3-FB_H-Crys and Crys-ADF3-FB_H-Crys gave much higher angle than bare

polystyrene surface. The experiment was repeated with two film preparation methods as explained in chapter 3.13: with ventilation to mimic the previous CA test and without ventilation to mimic the process of coating a well in 96-well plate (Figure 23).

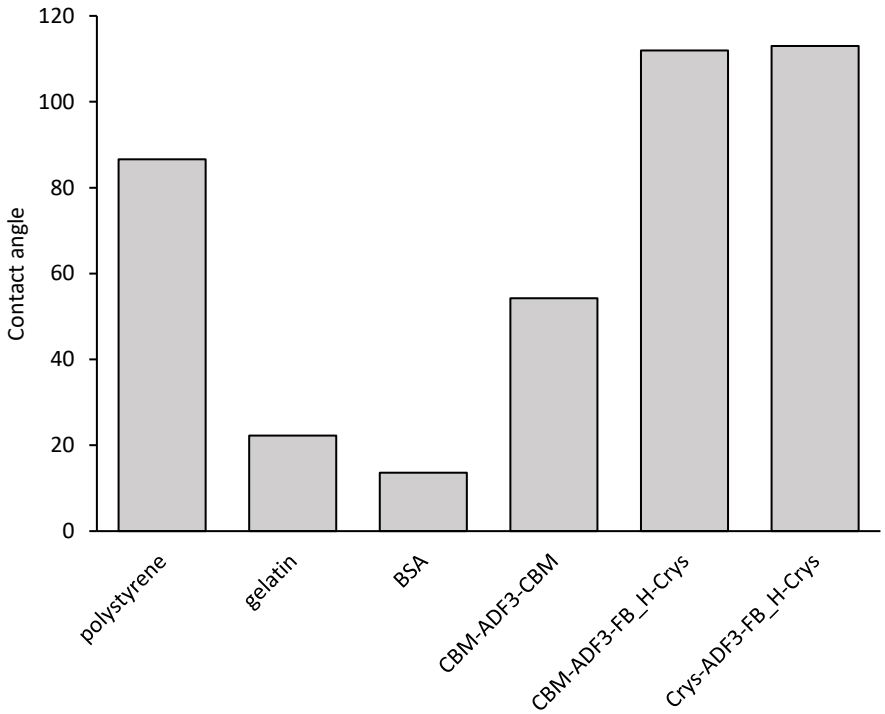

Figure 22. Water contact angle of silk films, test 1. Films were prepared on polystyrene surface by incubating 50 µl of 0.3 mg/ml protein solution overnight at room temperature with ventilation. Volume of water droplet in contact angle was 0.5-2 µl.

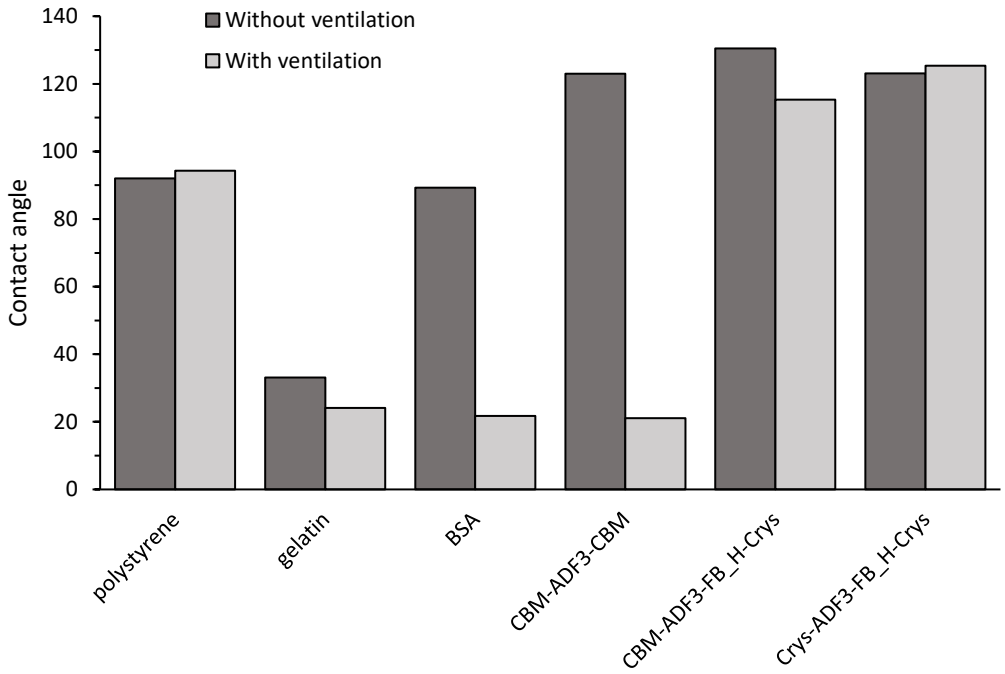

Figure 23. Water contact angle of silk films, test 2. Films were prepared on polystyrene surface with two methods; 50 µl of 0.3 mg/ml protein solution was incubated for 2 hours at room temperature without ventilation (lid closed), remaining solution was aspirated and then incubated overnight at room temperature, and with ventilation (lid open) where no liquid was aspirated. Volume of water droplet in contact angle was 0.5-2 µl.

4.5.2 Fourier-transform infrared spectroscopy

Results from FTIR are presented in Figure 24, and the recognized peak values in Table 3. Individual graphs can be found in attachments (Attachment 4, Attachment 5 and Attachment 6). Three protein structure sensitive bands were recognized as amide I (1610-1695 cm^{-1}), II (1480-1575 cm^{-1}) and III (1220-1320 cm^{-1}). Band at 1045 cm^{-1} is likely from TRIS (buffer) since absorption of C-N in RNH_2 gives band at 1030-1230 cm^{-1} and the three primary alcohols in TRIS exactly at 1050 cm^{-1}. Similarly, IR spectra of TRIS measured by Tan et al. had a high peak at around 1050 cm^{-1} [55]. This could be verified by measuring the spectra of the buffer. Water molecules give a wide band at 3000-3500 cm^{-1}, which overwhelms possible structural bands in that region, such as amide A and B. [53], [56]

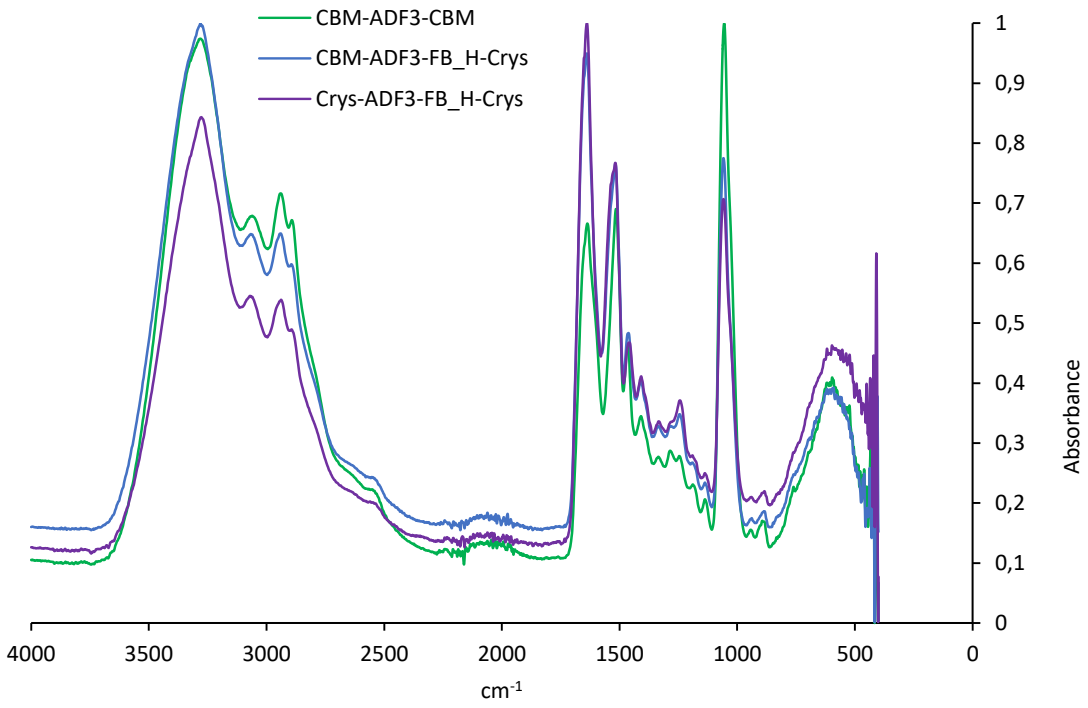

Figure 24. FTIR spectra of the silk constructs. Absorbances have been normalized. Recognized structural peaks: amide I ~1640 cm^{-1}, amide II ~1520 cm^{-1}, amide III ~1250-1240 cm^{-1}. Other peaks: water 3500-3000 cm^{-1} and TRIS ~1045 cm^{-1}.

Table 3. FTIR peak values of silk constructs.

Silk construct	Amide III	Amide II	Amide I	Unknown
CBM-ADF3-CBM	1636.7	1515.1	-	1055.3
CBM-ADF3-FB_H-Crys	1638.5	1517.5	1245.0	1058.5
Crys-ADF3-FB_H-Crys	1638.6	1518.2	1243.5	1058.6

5 Discussion

In this thesis three silk constructs were produced with cytotoxic LPS free *E. coli* strain (ClearColi BL21): CBM-ADF3-CBM, CBM-ADF3-FB_H-Crys and Crys-ADF3-FB_H-Crys. Cytotoxicity and biocompatibility in forms of cell viability and adhesion were tested with HDF cultivations on silk films and controls (gelatin, BSA, uncoated wells). The hypothesizes for structure-function relationships were that replacing CBM with gamma crystallin increases biocompatibility without lowering solubility, and addition of cell binding site increases cell adhesion. As seen in the results, cell viability did follow the hypothesis while cell adhesion did not. In addition, structures of different protein films were analyzed with FTIR and contact angle measurements, which did show structural similarities and surprisingly very hydrophobic water contact angles.

5.1 Production of silk like fusion proteins

The yield (Figure 7) and quality (Figure 8) of different batches indicate that induction earlier at log growth phase improved the yield of all three silk constructs at least by three fold, and reduced degradation of the silk. The improvement could also originate from media change from LB Lennox to Miller, but separate growth tests did not show any notable difference in OD_{600} between the two media. However, production with the optimized method has not been repeated and it is unknown if similar yields could be achieved again. The yield of CBM-ADF3-CBM is notably lower than the other two silk constructs, which could have been caused by many different factors, such as inefficient production of double CBM construct. Effect of gamma crystallin in solubility of the silk construct cannot be determined from these results, but the replacement of CBM with crystallin did have positive effect on the production yield. For further improvement in product yields, different IPTG concentrations and incubation times or EnPresso expression media could be tested. Genetic modifications, such as overexpressing tRNA pools are very time consuming to implement, and for small production batches of different silk constructs it would unlikely to save time.

5.2 Initial evaluation of cytotoxicity

The presented data (Figure 9, Figure 10, Figure 11, Figure 12 and Figure 13) lacks good quantitative properties. Counting cells from several small areas can lead to considerable errors since the cells are not evenly distributed. Thus, methods such as fluorescence assisted cell sorting should have been used for better quantitative data. Also, the images were taken from the end of the cultures and there is no proper data from the early cultures. Nevertheless, the HDF growth tests did not show notable cytotoxicity from the three silk constructs. While this was mostly expected due to previous research on spider silks [9]–[13], [44], [45] and origin of ɣ

crystallin, there has not been much research on cytotoxicity of cellulose binding module with exception of one study about binding bioactive molecules to cellulose via CBM, where the authors did not notice cytotoxic effects from CBM [57]. Surprisingly, no research was found on cytotoxicity of native ADF3 or its analogue eADF3. Due to the positive results, it was possible to move to viability and cell adhesions tests. It should be noted that the serum in culture mediums can mask negative effects of the matrix [58], e.g. poor cell adhesion or cytotoxicity, and thus cell culture tests should be done in serum-free medium to avoid false positive results.

5.3 Cell viability

All of the MTT results follow the same trend; the silk constructs show improvement in viability when moving from CBM terminal domains to ɣ-crystallin, although there is no significant difference between CBM-ADF3-CBM and CBM-ADF3-FB_H-CBM. In comparison to control, BSA and gelatin, Crys-ADF3-FB_H-Crys supported similar or a bit higher cell viability than gelatin while BSA and CBM-ADF3-CBM were on the same level with each other. Control (uncoated wells) had high variety between the measurements for unknown reason, but overall it could be considered to be similar with BSA and CBM-ADF3-CBM. Gelatin is hydrolyzed collagen, which is the primary component of the ECM type that is habited by fibroblasts. Collagen contains functional groups and adhesion domains suitable for HDF that are likely to be present in gelatin [59]. Thus, it is very promising for Crys-ADF3-FB_H-Crys to support as good or even higher cell viability than gelatin.

However, the results did not exclusively come from NADH level of individual cells. During experiments it was noticed that the density of properly adhered cells prior to MTT staining had very high effect on the result and there was no notable difference in absorbance between similar cell densities. Thus, the MTT result was coupled with cell adhesion and it is possible that it completely outweighed the difference in amount of NADH in individual cells. This does not make the experiment meaningless as the results can still be used to evaluate the overall cell viability in the scaffold material, which is dominated by the capacity of supporting cell attachment and growth. In addition, similar correlations with viability assay absorbance and adhered cells were found in other articles [13], [60].

5.4 Cell adhesion

The cell adhesion results from both tests (Figure 20 and Figure 21) were very similar. Of the three silk constructs Crys-ADF3-FB_H-Crys achieved highest values while CBM-ADF3-CBM and CBM-ADF3-FB_H-Crys were close to each other. The hypothesis was that the addition of fibronectin binding site would show notable improvement in cell adhesion, which was not seen here. The results indicated that the binding site was not accessible at least in CBM-ADF3-FB_H-

Crys. Accessibility of the site in Crys-ADF3-FB_H-Crys could be tested by repeating the assay with additional silk construct Crys-ADF3-Crys. Alternatively, it is possible that the binding site was not compatible with HDF. The research group that identified the binding site tested it with human embryonic stem cells and no literature was found on fibroblast adhesion to it [26]. Still, considering that the cells were not able to adhere onto the uncoated polystyrene wells, all of the silk constructs did show significant increase in cell adhesion.

Since the MTT result was noted to be tied with cell adhesion, it was surprising for gelatin to show better cell adhesion than Crys-ADF3-FB_H-Crys, indicating that the MTT result was not completely overwhelmed by adhesion properties as suggested earlier. BSA was found to be non-adhesion protein that can be used as an additive in some adhesion protein coatings (gelatin, fibronectin) [61], [62]. Thus, poor adhesion on BSA was not surprising, but it also did not give any additional information, and could be left out in further experiments.

5.5 Structural analysis of silk films

The water contact angle results (Figure 22 and Figure 23) were roughly repeatable with the exception of CBM-ADF3-CBM CA decreasing from 54 degrees to 21. Silks constructs CBM-ADF3-FB_H-Crys and Crys-ADF3-FB_H-Crys achieved very high CA (113.0°-130.5°) with both preparation methods, while CA of CBM-ADF3-CBM and BSA changed significantly with different preparation method. With BSA the change assumedly came from low amount of protein in the films, as there was barely any difference to CA of polystyrene and the BSA films were very difficult to see. However, in CBM-ADF3-CBM there seemed to be very fundamental structural changes. The results would suggest that the high hydrophobicity came from ADF3 as all silk construct did achieve high CA, and at least in case of CBM-ADF3-CBM it was possible to alter the hydrophobicity to hydrophilicity by changing the preparation method of the film. It is unknown what could cause the change in CA or the high CA in silk films. One explanation could be that the hydrophobic alanine blocks of ADF3 stacked at the surface forming a hydrophobic layer, which could have been caused by evaporation of water forcing hydrophilic (amorphous) regions to group together.

High CA with water is associated with charged surface chemistry and/or surface morphology. 90° contact angle with water is considered hydrophobic and 150° as superhydrophobic. High hydrophobicity is unusual in natural biomaterials, and thus synthetic biomaterials are often used in biomedical applications that require hydrophobicity. Cells have been shown to prefer rough surfaces, but there is no clear connection between surface chemistry and cell adhesion and proliferation. Some authors have noted enhancement of biocompatibility when increasing hydrophobicity while other authors have reported the opposite reaction, which indicates that different cell types prefer surfaces with particular hydrophobicity (/-

philicity). [63], [64] Since it is unknown how the surface morphology behaves when wetted with culture medium, it is not possible to draw accurate structure-function relationships between cell adhesion and surface morphology or chemistry from just the CA of dry film with water droplet. It can be said that there is no notable connection between CA of dry film and cell viability or adhesion. It should be noted that the films were unlikely to be homogeneous, and there could have been air pockets on the surface affecting its properties.

The silk films were analyzed with FTIR (Figure 24), and amide I, II and III peaks were identified. Evaluation of α-helix or β-sheet content was not done here as it would require more in-depth analyzation in order to explain structural relationship with amide band peak locations. Still, the results indicate that the three silk constructs had very similar structures. Crys-ADF3-FB_H-Crys and CBM-ADF3-FB_H-Crys gave almost identical spectra while CBM-ADF3-CBM had lower (relative) amide I and II intensity and no notable amide III peak. This could have been caused by the absence of ɣ-crystallin, rather than difference in secondary structure of ADF3. The peak shifts of amide bands I, II and III (Table 3) were very small between the silk constructs and possibly within the resolution of the FTIR instrument, which also supports similarity of the secondary structures. [53], [56]

6 Conclusion

Three silk like fusion proteins, CBM-ADF3-CBM, CBM-ADF3-FB_H-Crys and Crys-ADF3-FB_H-Crys, with central unit spidroin ADF3 by *A. diadematus* were produced with cytotoxic LPS free *E. coli* strain, and purified with FPLC. The purified silk protein concentrates were used to coat glass slides and polystyrene wells for cytotoxicity and biocompatibility tests, respectively. Cytotoxicity tests were performed with over week long HDF cultivations. Biocompatibility with HDF was tested in forms of cell viability and cell adhesion with two day MTT experiments and four hour cell adhesion assays, respectively. Controls for all previous experiments were uncoated well, BSA and gelatin. The structures of the silk films were analyzed with FTIR and contact angle measurements with water on coated polystyrene surface.

The silk protein production protocol was optimized to increase the yield and in the final batch yields 6.5 mg/L, 15.2 mg/L and 15.3 mg/L were achieved for CBM-ADF3-CBM, CBM-ADF3-FB_H-Crys and Crys-ADF3-FB_H-Crys, respectively, which was over three fold increase to previous batches. In cytotoxicity test there was no notable difference in cell densities between controls (glass slide, gelatin, BSA) and silk films, indicating absence of cytotoxicity in any of the silk constructs. The cell viability test showed increase in absorbance, i.e. viability, when moving from CBM terminals to crystallin, which was in accord with the hypothesis. Cell viability with Crys-ADF3-FB_H-Crys was higher than gelatin in all tests (significant in half of the tests, α=0.05), which is very promising considering that gelatin is partly hydrolyzed collagen, the main component of fibroblast ECM. In cell adhesion assays the adhesion was not notably different between CBM-ADF3-CBM and CBM-ADF3-FB_H-Crys, indicating that the adhesion site was not accessible or compatible with HDF. The adhesion was increased significantly in Crys-ADF3-FB_H-Crys, but it is unknown whether this comes from better accessibility to the site or from the presence of crystallin. Unlike in cell viability tests, gelatin achieved higher results than Crys-ADF3-FB_H-Crys, assumedly because of the fibroblast adhesion sites.

The FTIR analysis of silk films showed high structural similarity between the silk constructs, albeit with some differences in relative peak intensities and absence of clear amide III peak in CBM-ADF3-CBM. Contact angle measurements were performed with and without ventilation during 2-hour incubation of the protein films followed by aspiration of the remaining solution, where the latter mimics the coating of 96-well plate. Surprisingly, contact angles of the silk constructs were mostly very hydrophobic (112.0-130.5°), with exception of ventilated CBM-ADF3-CBM silk films (21.0-54.2°). The results suggest that the high hydrophobicity came from ADF3, and at least with CBM-ADF3-CBM the hydrophobicity could be altered drastically by increasing protein layer thickness and/or slowly evaporating

the water. While the causes of these results are unknown, one explanation could be that the hydrophobic alanine blocks of ADF3 stacked at the surface forming a hydrophobic layer due to slow evaporation of water that forced the hydrophilic (amorphous) regions to group together.

The aim of this thesis was to evaluate cytotoxicity and biocompatibility of ADF3 fusion proteins and draw conclusions about structure-function relationship, and compare the silk materials to conventional materials. These goals were achieved. However, the given silk constructs and methods were not enough to fully explain the structure-function relationship of CBM/crystallin and heparin cell adhesion site to biocompatibility. For future work, silk constructs, such as CBM-ADF3-FB_H-CBM, CBM-ADF3-Crys and Crys-ADF3-Crys could answer these questions. Also, silk construct with fibronectin domains, culturing with stem cell lines and modification of silk films with kosmotropic salts could be used to widen the research.

References

[1] F. J. O'Brien, "Biomaterials & scaffolds for tissue engineering," *Materials Today*, vol. 14, no. 3, pp. 88–95, 2011.

[2] D. Huemmerich, U. Slotta, and T. Scheibel, "Processing and modification of films made from recombinant spider silk proteins," *Applied Physics A: Materials Science and Processing*, vol. 82, no. 2, pp. 219–222, 2006.

[3] A. Rising and J. Johansson, "Toward spinning artificial spider silk," *Nature Chemical Biology*. 2015.

[4] K. Spiess, A. Lammel, and T. Scheibel, "Recombinant spider silk proteins for applications in biomaterials," *Macromolecular Bioscience*. 2010.

[5] M. Heim, D. Keerl, and T. Scheibel, "Spider silk: From soluble protein to extraordinary fiber," *Angewandte Chemie - International Edition*, vol. 48, no. 20. pp. 3584–3596, 2009.

[6] H. Chung, T. Y. Kim, and S. Y. Lee, "Recent advances in production of recombinant spider silk proteins," *Current Opinion in Biotechnology*, vol. 23, no. 6. pp. 957–964, 2012.

[7] X.-X. Xia, Z.-G. Qian, C. S. Ki, Y. H. Park, D. L. Kaplan, and S. Y. Lee, "Native-sized recombinant spider silk protein produced in metabolically engineered Escherichia coli results in a strong fiber," *Proceedings of the National Academy of Sciences*, vol. 107, no. 32, pp. 14059–14063, 2010.

[8] M. Widhe, J. Johansson, M. Hedhammar, and A. Rising, "Invited review: Current progress and limitations of spider silk for biomedical applications," *Biopolymers*. 2012.

[9] M. M. Moisenovich *et al.*, "In vitro and in vivo biocompatibility studies of a recombinant analogue of spidroin 1 scaffolds," *Journal of Biomedical Materials Research - Part A*, 2011.

[10] L. Baoyong, Z. Jian, C. Denglong, and L. Min, "Evaluation of a new type of wound dressing made from recombinant spider silk protein using rat models," *Burns*, 2010.

[11] M. Stark *et al.*, "Macroscopic fibers self-assembled from recombinant miniature spider silk proteins," *Biomacromolecules*, 2007.

[12] C. Fredriksson *et al.*, "Tissue response to subcutaneously implanted recombinant spider silk: An in vivo study," *Materials*, 2009.

[13] M. Widhe, N. D. Shalaly, and M. Hedhammar, "A fibronectin mimetic motif improves integrin mediated cell biding to recombinant spider silk matrices," *Biomaterials*, 2016.

[14] V. P. R. Vendra, I. Khan, S. Chandani, A. Muniyandi, and D. Balasubramanian, "Gamma crystallins of the human eye lens," *Biochimica et Biophysica Acta - General Subjects*, 2016.

[15] R. O. Hynes, “The extracellular matrix: Not just pretty fibrils,” *Science*, vol. 326, no. 5957. pp. 1216–1219, 2009.

[16] S. F. Badylak, “The extracellular matrix as a scaffold for tissue reconstruction,” *Seminars in Cell & Developmental Biology*, vol. 13, no. 5, pp. 377–383, 2002.

[17] R. O. Hynes and A. Naba, “Overview of the matrisome-An inventory of extracellular matrix constituents and functions,” *Cold Spring Harbor Perspectives in Biology*, vol. 4, no. 1, 2012.

[18] BioNinja, “Extracellular matrix.” [Online]. Available: http://ib.bioninja.com.au/standard-level/topic-1-cell-biology/13-membrane-structure/extracellular-matrix.html. [Accessed: 13-Sep-2018].

[19] B. Alberts *et al.*, *Molecular Biology of the Cell 6e*, vol. 6, no. 6. 2014.

[20] D. J. S. Hulmes, “Collagen diversity, synthesis and assembly,” in *Collagen: Structure and Mechanics*, 2008, pp. 15–47.

[21] S. P. Canelón and J. M. Wallace, “β-Aminopropionitrile-induced reduction in enzymatic crosslinking causes in vitro changes in collagen morphology and molecular composition,” *PLoS ONE*, 2016.

[22] S. Yang, K.-F. Leong, Z. Du, and C.-K. Chua, “The Design of Scaffolds for Use in Tissue Engineering. Part I. Traditional Factors,” *Tissue Engineering*, 2001.

[23] J. D. Humphries, “Integrin ligands at a glance,” *Journal of Cell Science*, 2006.

[24] E. Ruoslahti, “RGD AND OTHER RECOGNITION SEQUENCES FOR INTEGRINS,” *Annual Review of Cell and Developmental Biology*, 1996.

[25] C. Mas-Moruno, F. Rechenmacher, and H. Kessler, “Cilengitide: The First Anti-Angiogenic Small Molecule Drug Candidate. Design, Synthesis and Clinical Evaluation,” *Anti-Cancer Agents in Medicinal Chemistry*, 2010.

[26] J. R. Klim, L. Li, P. J. Wrighton, M. S. Piekarczyk, and L. L. Kiessling, “A defined glycosaminoglycan-binding substratum for human pluripotent stem cells,” *Nature Methods*, 2010.

[27] B. P. Orner, R. Derda, R. L. Lewis, J. A. Thomson, and L. L. Kiessling, “Arrays for the combinatorial exploration of cell adhesion,” *Journal of the American Chemical Society*, 2004.

[28] J. R. Jones, “Reprint of: Review of bioactive glass: From Hench to hybrids,” *Acta Biomaterialia*. 2015.

[29] L. S. Nair and C. T. Laurencin, “Biodegradable polymers as biomaterials,” *Progress in Polymer Science (Oxford)*. 2007.

[30] M. C. Gomez-Guillen, B. Gimenez, M. E. Lopez-Caballero, and M. P. Montero, “Functional and bioactive properties of collagen and gelatin from

alternative sources: A review," *Food Hydrocolloids*. 2011.

[31] H. K. Kleinman and G. R. Martin, "Matrigel: Basement membrane matrix with biological activity," *Seminars in Cancer Biology*, 2005.

[32] W. W. Thein-Han, Y. Kitiyanant, and R. D. K. Misra, "Chitosan as scaffold matrix for tissue engineering," *Materials Science and Technology*, 2008.

[33] J. Sun and H. Tan, "Alginate-based biomaterials for regenerative medicine applications," *Materials*. 2013.

[34] W. Huang, S. Ling, C. Li, F. G. Omenetto, and D. L. Kaplan, "Silkworm silk-based materials and devices generated using bio-nanotechnology," *Chemical Society Reviews*, 2018.

[35] J. C. V. Ribeiro, R. S. Vieira, I. M. Melo, V. M. A. Araújo, and V. Lima, "Versatility of Chitosan-Based Biomaterials and Their Use as Scaffolds for Tissue Regeneration," *Scientific World Journal*. 2017.

[36] S. Gomes, I. B. Leonor, J. F. Mano, R. L. Reis, and D. L. Kaplan, "Natural and genetically engineered proteins for tissue engineering," *Progress in Polymer Science (Oxford)*, 2012.

[37] R. Jansson, "Strategies for Functionalization of Recombinant Spider Silk," Swedish University of Agricultural Sciences, 2015.

[38] E. Luong-Van, L. Grøndahl, K. N. Chua, K. W. Leong, V. Nurcombe, and S. M. Cool, "Controlled release of heparin from poly(epsilon-caprolactone) electrospun fibers.," *Biomaterials*, 2006.

[39] M. Andersson, J. Johansson, and A. Rising, "Silk spinning in silkworms and spiders," *International Journal of Molecular Sciences*. 2016.

[40] N. A. Ayoub, J. E. Garb, R. M. Tinghitella, M. A. Collin, and C. Y. Hayashi, "Blueprint for a High-Performance Biomaterial: Full-Length Spider Dragline Silk Genes," *PLoS ONE*, 2007.

[41] K. Schacht and T. Scheibel, "Processing of recombinant spider silk proteins into tailor-made materials for biomaterials applications," *Current Opinion in Biotechnology*. 2014.

[42] M. Lewicka, O. Hermanson, and A. U. Rising, "Recombinant spider silk matrices for neural stem cell cultures," *Biomaterials*, 2012.

[43] P. Bhattacharjee *et al.*, "Silk scaffolds in bone tissue engineering: An overview," *Acta Biomaterialia*. 2017.

[44] S. Wohlrab *et al.*, "Cell adhesion and proliferation on RGD-modified recombinant spider silk proteins," *Biomaterials*, 2012.

[45] K. Schacht, T. Jüngst, M. Schweinlin, A. Ewald, J. Groll, and T. Scheibel, "Biofabrication of cell-loaded 3D spider silk constructs," *Angewandte Chemie - International Edition*, 2015.

[46] A. Florczak, A. Mackiewicz, and H. Dams-Kozlowska, "Functionalized

spider silk spheres as drug carriers for targeted cancer therapy," *Biomacromolecules*, 2014.

[47] R. Jansson *et al.*, "Recombinant spider silk genetically functionalized with affinity domains," *Biomacromolecules*, 2014.

[48] Lucigen, "ClearColi® BL21(DE3) Electrocompetent Cells." [Online]. Available: https://www.lucigen.com/ClearColi-BL21-DE3-Electrocompetent-Cells/#subcat-tabs3. [Accessed: 10-Sep-2018].

[49] L. E. Tracy, R. A. Minasian, and E. J. Caterson, "Extracellular Matrix and Dermal Fibroblast Function in the Healing Wound," *Advances in Wound Care*, 2016.

[50] Sigma Aldrich, "Human Dermal Fibroblasts (HDF) Culture Protocol." [Online]. Available: http://www.sigmaaldrich.com/technical-documents/protocols/biology/human-dermal-fibroblasts.printerview.html. [Accessed: 17-Aug-2018].

[51] S. A. Ock and G. J. Rho, "Effect of dimethyl sulfoxide (DMSO) on cryopreservation of porcine mesenchymal stem cells (pMSCS)," *Cell Transplantation*, 2011.

[52] J. Van Meerloo, G. J. L. Kaspers, and J. Cloos, "Cell sensitivity assays: The MTT assay," *Methods in Molecular Biology*, 2011.

[53] J. M. Fabian, H. , Mäntele, W. and Chalmers, *Infrared Spectroscopy of Proteins. In Handbook of Vibrational Spectroscopy*. 2006.

[54] A. Osahor, K. Deekonda, L. C. Weng, E. U. H. Sim, A. Radu, and K. Narayanan, "Rapid preparation of adherent mammalian cells for basic scanning electron microscopy (SEM) analysis," *Analytical Biochemistry*, 2017.

[55] H. Tan, J. Wu, and Y. Chen, "Terbium(III) based coordination polymer microparticles as a luminescent probe for ascorbic acid," *Microchimica Acta*, 2014.

[56] T. Hase, *Tables for organic spectrometry*, 10th ed. Otatieto, 2008.

[57] F. K. Andrade, R. Costa, L. Domingues, R. Soares, and M. Gama, "Improving bacterial cellulose for blood vessel replacement: Functionalization with a chimeric protein containing a cellulose-binding module and an adhesion peptide," *Acta Biomaterialia*, 2010.

[58] M. Widhe *et al.*, "Recombinant spider silk as matrices for cell culture," *Biomaterials*, 2010.

[59] N. Davidenko *et al.*, "Evaluation of cell binding to collagen and gelatin: a study of the effect of 2D and 3D architecture and surface chemistry," *Journal of Materials Science: Materials in Medicine*, 2016.

[60] M. Widhe, U. Johansson, C. O. Hillerdahl, and M. Hedhammar, "Recombinant spider silk with cell binding motifs for specific adherence of

cells," *Biomaterials*, 2013.

[61] M. Kan, Y. Minamoto, S. Sunami, I. Yamam, and M. Umeda, "The effects on cell adhesion of fibronectin and gelatin in a serum-free, bovine serum albumin medium.," *Cell Structure and Function*, vol. 7, no. 3, pp. 245–252, 1982.

[62] J. E. Koblinski, "Matrix cell adhesion activation by non-adhesion proteins," *Journal of Cell Science*, 2005.

[63] D. P. Dowling, I. S. Miller, M. Ardhaoui, and W. M. Gallagher, "Effect of surface wettability and topography on the adhesion of osteosarcoma cells on plasma-modified polystyrene," *Journal of Biomaterials Applications*, 2011.

[64] F. Dong, M. Zhang, W. Huang, L. Zhou, M. S. Wong, and Y. Wang, "Superhydrophobic/hydrophobic nanofibrous network with tunable cell adhesion: Fabrication, characterization and cellular activities," *Colloids and Surfaces A: Physicochemical and Engineering Aspects*, 2015.

Attachments

Attachment 1.SEM: Fibroblast culture on glass.

Attachment 2. SEM: Fibroblast culture on glass.

Attachment 3. SEM: Fibroblast culture on CMB-ADF3-CBM film.

Attachment 4. FTIR spectra of CBM-ADF3-CBM film.

Attachment 5. FTIR spectra of CBM-ADF3-FB_H-Crys film.

Attachment 6. FTIR spectra of Crys-ADF3-FB_H-Crys film.

Attachment 1.SEM: Fibroblast culture on glass.

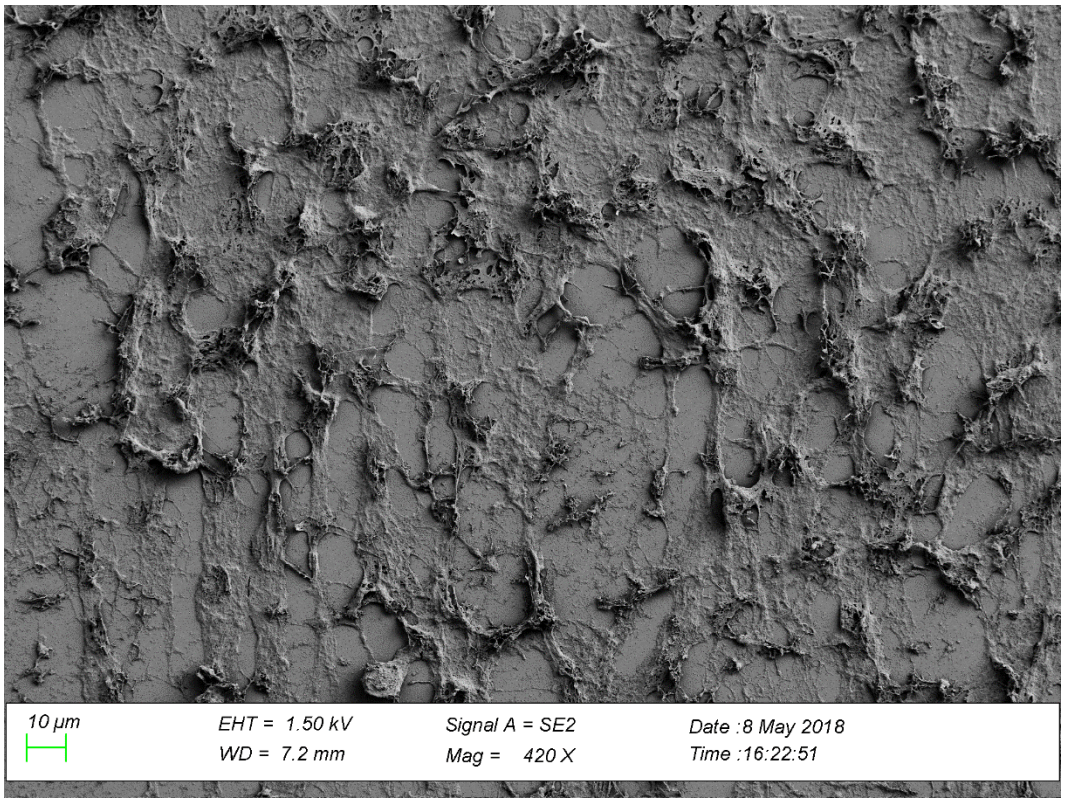

Attachment 2. SEM: Fibroblast culture on glass.

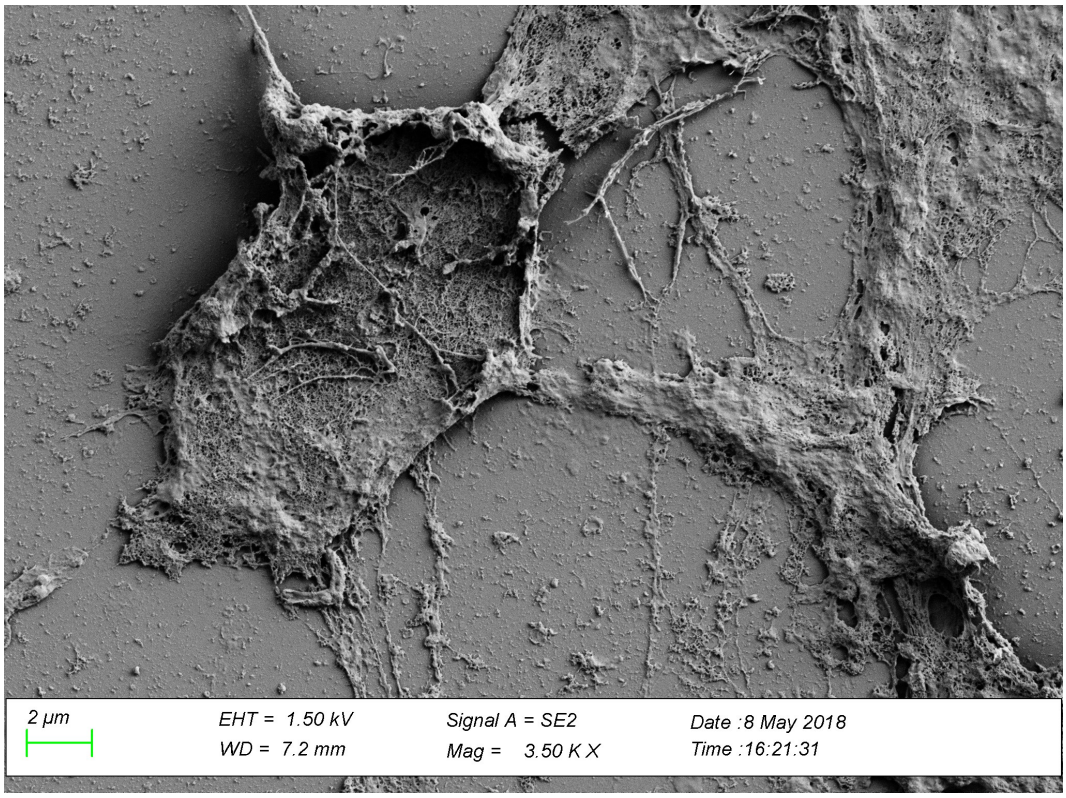

Attachment 3. SEM: Fibroblast culture on CMB-ADF3-CBM film.

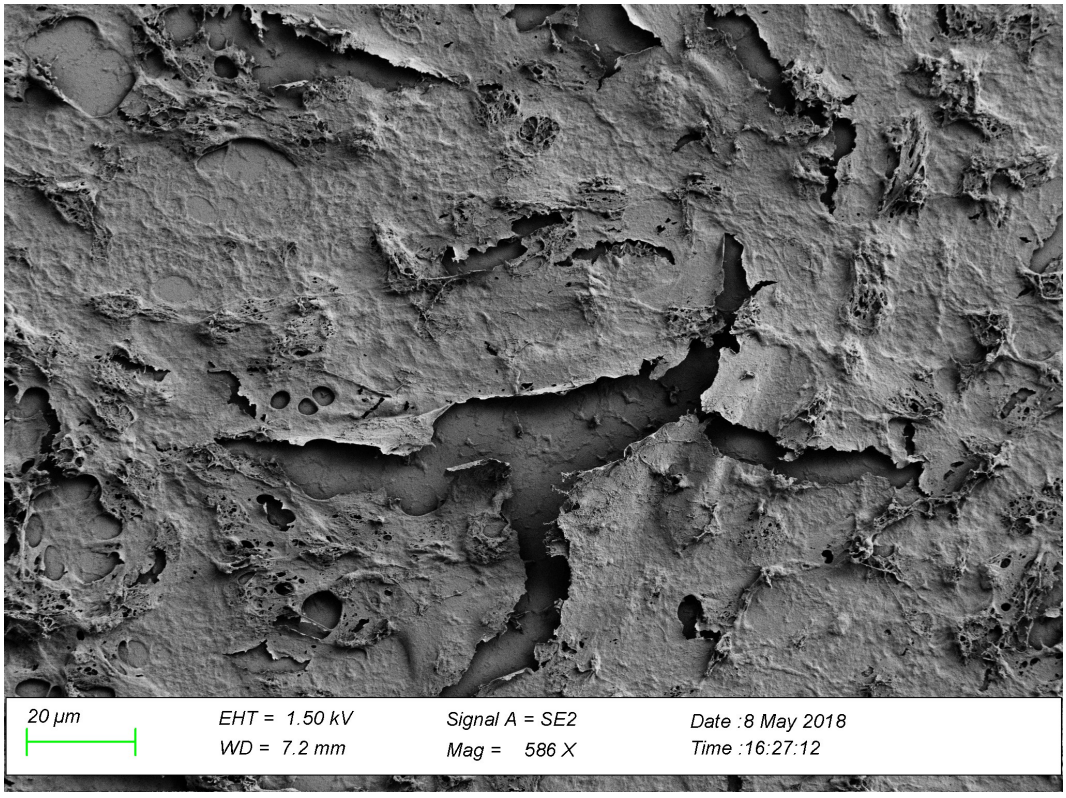

Attachment 4. FTIR spectra of CBM-ADF3-CBM film. Absorbance has been normalized. Recognized structural peaks: amide I ~1640 cm^{-1}, amide II ~1520 cm^{-1}, amide III ~1250-1240 cm^{-1}. Other peaks: water 3500-3000 cm^{-1} and TRIS ~1045 cm^{-1}.

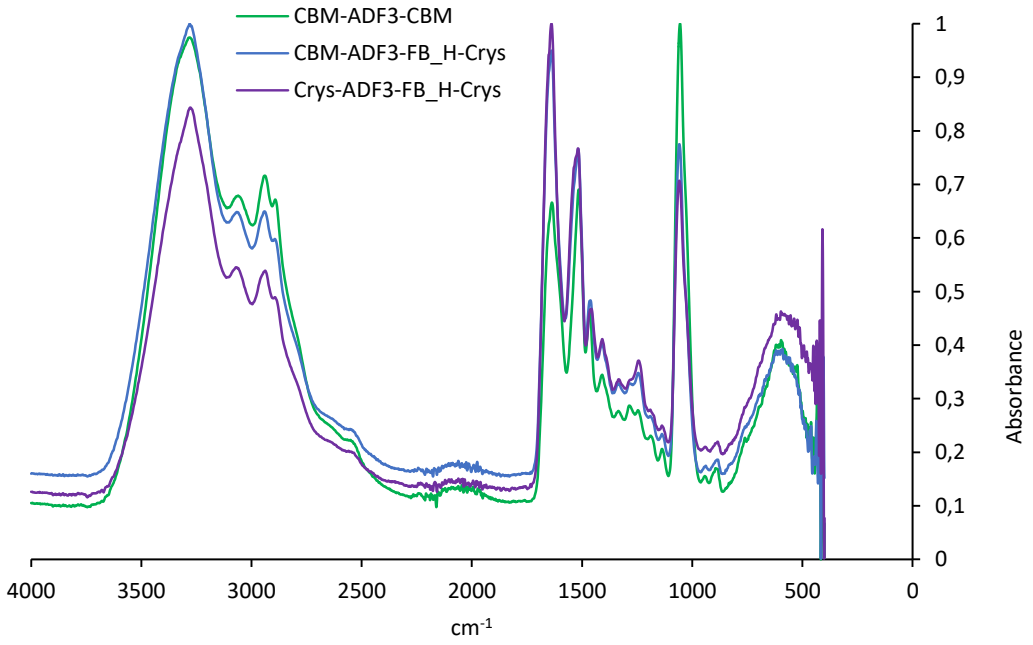

Attachment 5. FTIR spectra of CBM-ADF3-FB_H-Crys film. Absorbance has been normalized. Recognized structural peaks: amide I ~1640 cm^{-1}, amide II ~1520 cm^{-1}, amide III ~1250-1240 cm^{-1}. Other peaks: water 3500-3000 cm^{-1} and TRIS ~1045 cm^{-1}.

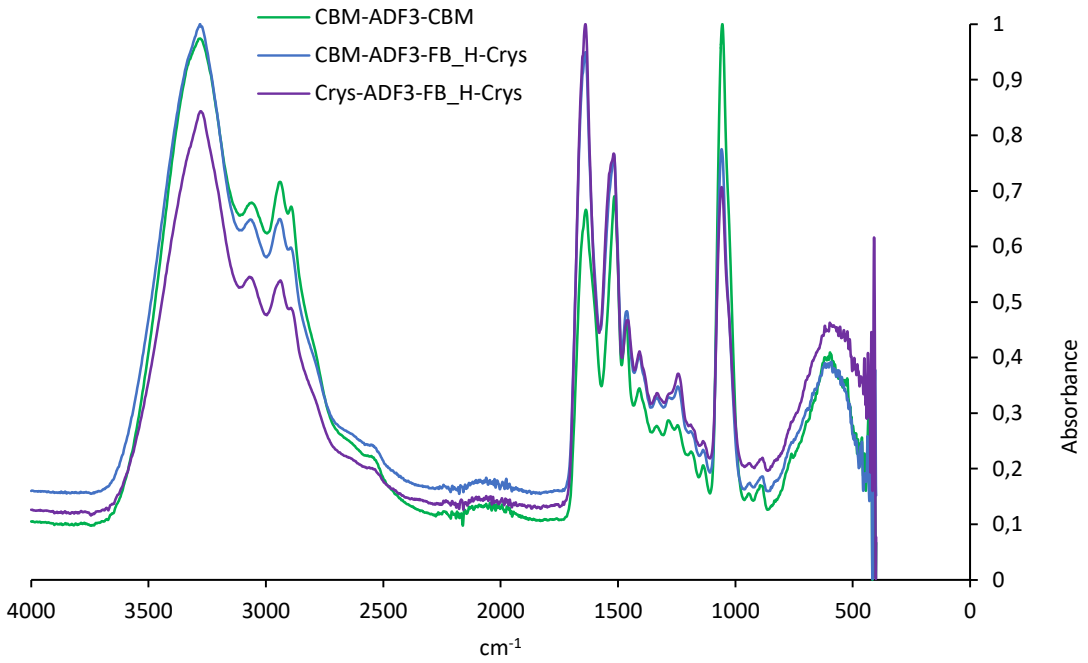

Attachment 6. FTIR spectra of Crys-ADF3-FB_H-Crys film. Absorbance has been normalized. Recognized structural peaks: amide I ~1640 cm^{-1}, amide II ~1520 cm^{-1}, amide III ~1250-1240 cm^{-1}. Other peaks: water 3500-3000 cm^{-1} and TRIS ~1045 cm^{-1}.